

**DEVELOPMENT AND ROBUST CONTROLLER DESIGN
FOR UNDERACTUATED UNDERWATER GLIDER
PLATFORM FOR UMP LAKE MONITORING**



DR. MAZIYAH MAT NOH

DR. ZAINAH MD ZAIN

DR. DWI PEBRIANTI

DR. ADDIE IRAWAN HASHIM

DR MOHD RAZALI DAUD

RESEARCH VOT NO:

UMP
RDU1303117

Faculty of Electrical & Electronics Engineering

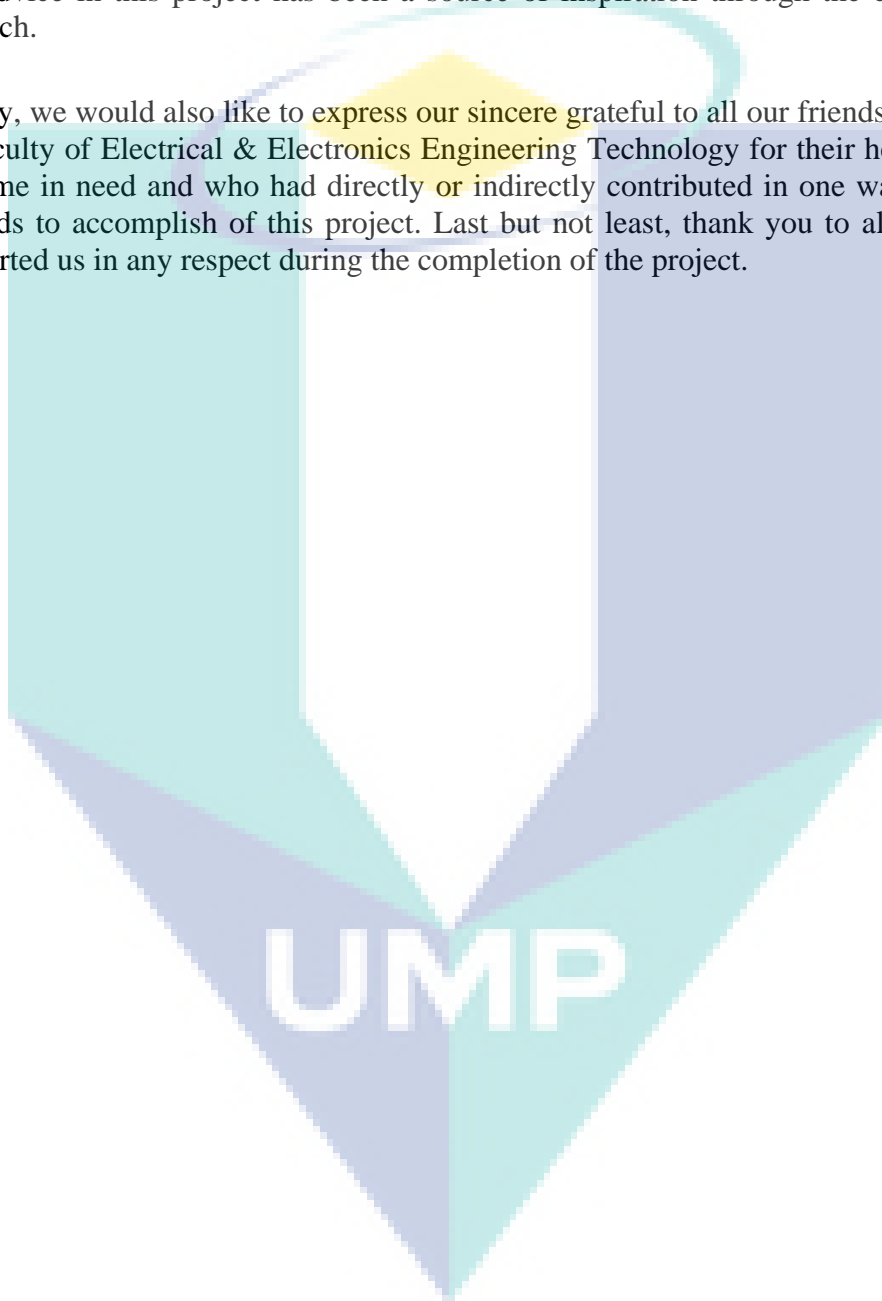
UNIVERSITI MALAYSIA PAHANG

2016

ACKNOWLEDGEMENTS

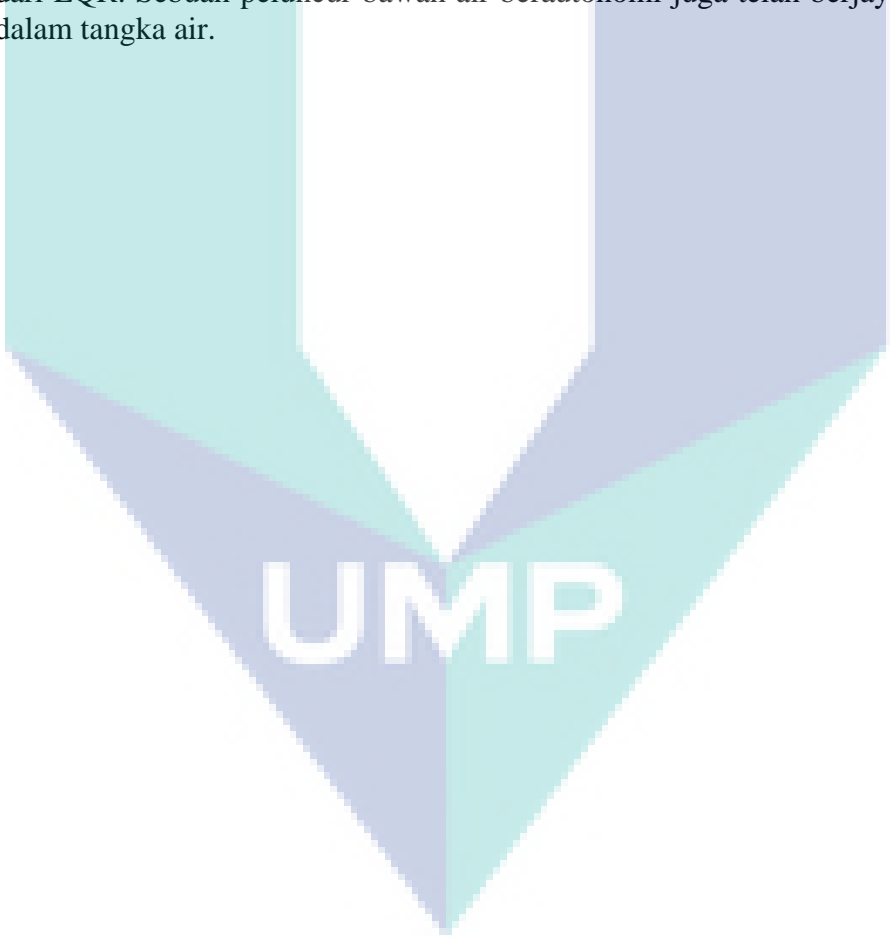
First of all, thanks to Allah SWT on His blessing to make this research successful. Million thankful and appreciation to all research mates, whose encouragement, guidance and support from the initial to the final level with patience and knowledge enabled this group to develop an understanding of the project. The invaluable guidance and advice in this project has been a source of inspiration through the course of this research.

Finally, we would also like to express our sincere grateful to all our friends and students of Faculty of Electrical & Electronics Engineering Technology for their helping during the time in need and who had directly or indirectly contributed in one way or another towards to accomplish of this project. Last but not least, thank you to all that always supported us in any respect during the completion of the project.



ABSTRAK

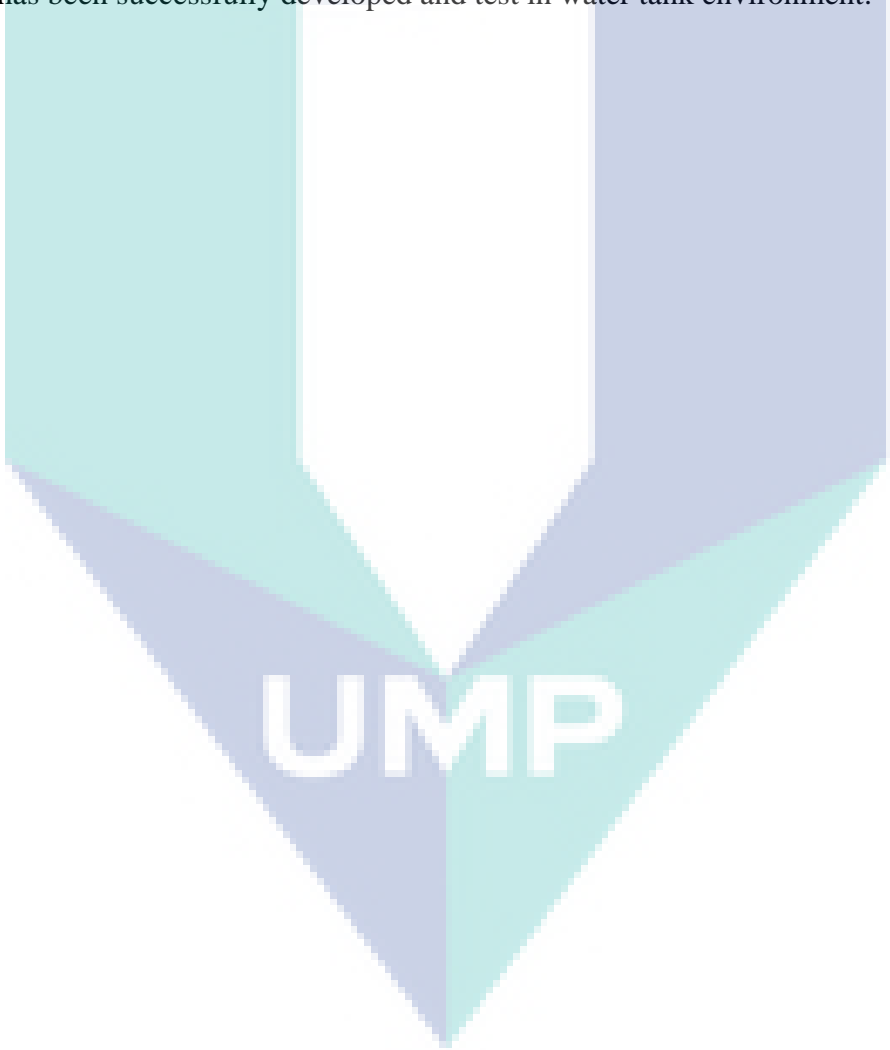
Peluncur bawah air berautonomi (AUG) yang merupakan sejenis kenderaan bawah air berautonomi (AUV) yang mempunyai penggerak yang terhad. Atas sebab ini, objektif utama penyelidikan ini adalah untuk membina hukum kawalan yang mempunyai keupayaan dalam menghadapi gangguan luar dan ketidakpastian akibat pekali hidrodinamik. Oleh itu, pengawal tegar tak lurus telah direka dengan menggunakan algoritma pengawal kawalan mod gelanggar. Oleh itu, objektif utama kajian ini adalah untuk merekabentuk dan membangunkan algoritma pengawal yang membuatkan peluncur boleh suai walaupun menghadapi kekangan-kekangan ini. Satu pengawal kawalan mod gelanggar (QSMC) yang kukuh dan boleh diharap telah direka untuk tujuan ini. Pengawal ini dapat menyesuaikan diri terhadap keadaan perubahan yang dinamik dan mampu untuk pampas gangguan dari arus air. Berdasarkan keputusan simulasi penandaarasan kaedah kawalan mod gelanggar telah berjaya mencapai bacaan yang diinginkan. Prestasi QSMC telah dibandingkan dengan pengatur linear kuadratik(LQR). Secara keseluruhan, QSMC menunjukkan prestasi dua kali ganda lebih dari LQR. Sebuah peluncur bawah air berautonomi juga telah berjaya dibina dan di uji dalam tangka air.

The logo of UMPA (Universiti Malaysia Perlis) is a large, downward-pointing arrow shape. It is composed of four triangular sections meeting at a central point. The top-left and bottom-right sections are light blue, while the top-right and bottom-left sections are a slightly darker shade of blue. The letters 'UMPA' are written in a bold, white, sans-serif font across the center of the arrow.

UMPA

ABSTRACT

The autonomous underwater glider (AUG) demonstrates highly nonlinear and complexity in its dynamic model and also coupled with external underwater environment and disturbance. With limited actuators, the only option that AUG has in facing such environment and disturbances is by using strategies of control algorithm. For this reason, the main objective of this research is to formulate the control law that has the capability in facing the external disturbances and uncertainties due its hydrodynamics coefficients. As a result, a robust and reliable has been designed using quasi sliding mode control algorithm (QSMC) for the linearised model of longitudinal plane of an AUG. The performance of QSMC has been compared to linear quadratic regulator (LQR). The simulation results have shown that the proposed controller provides the smallest two times faster settling time than LQR. The prototype of the AUG has been successfully developed and test in water tank environment.



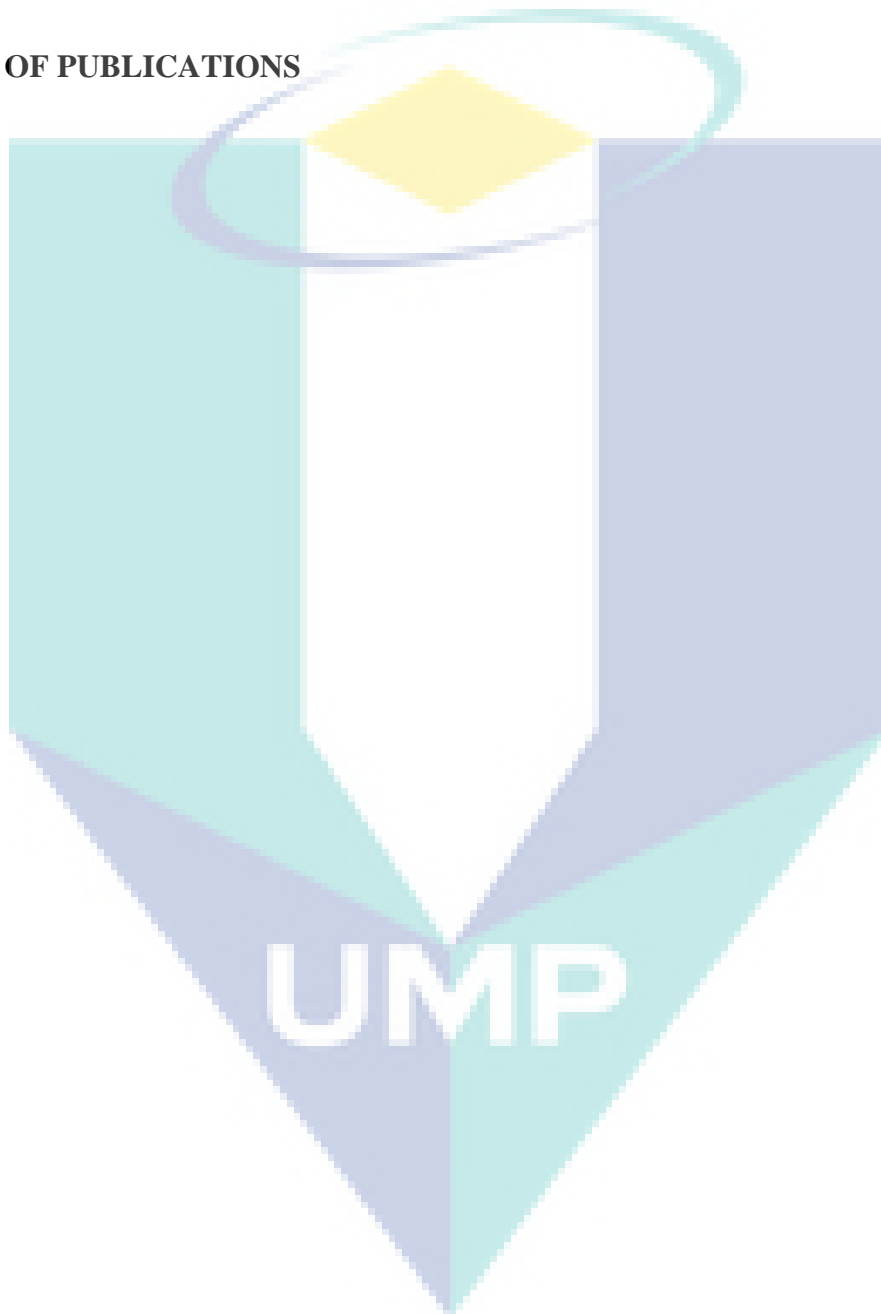
UMP

TABLE OF CONTENT

DECLARATION	
TITLE PAGE	
ACKNOWLEDGEMENTS	ii
ABSTRAK	iii
ABSTRACT	iv
TABLE OF CONTENT	v
LIST OF TABLES	viii
LIST OF FIGURES	ix
LIST OF SYMBOLS	xi
LIST OF ABBREVIATIONS	xiii
CHAPTER 1 INTRODUCTION	1
1.1 Background	1
1.2 Problem Statement	3
1.3 Research Objectives	3
CHAPTER 2 LITERATURE REVIEW	4
2.1 Introduction	4
2.2 Control Strategies	4
2.2.1 Linear Control Strategies	5
2.2.2 Nonlinear Control Strategies	6
2.2.3 Intelligent Control Strategies	8
2.3 Autonomous Underwater Glider Designs and Characteristics	9

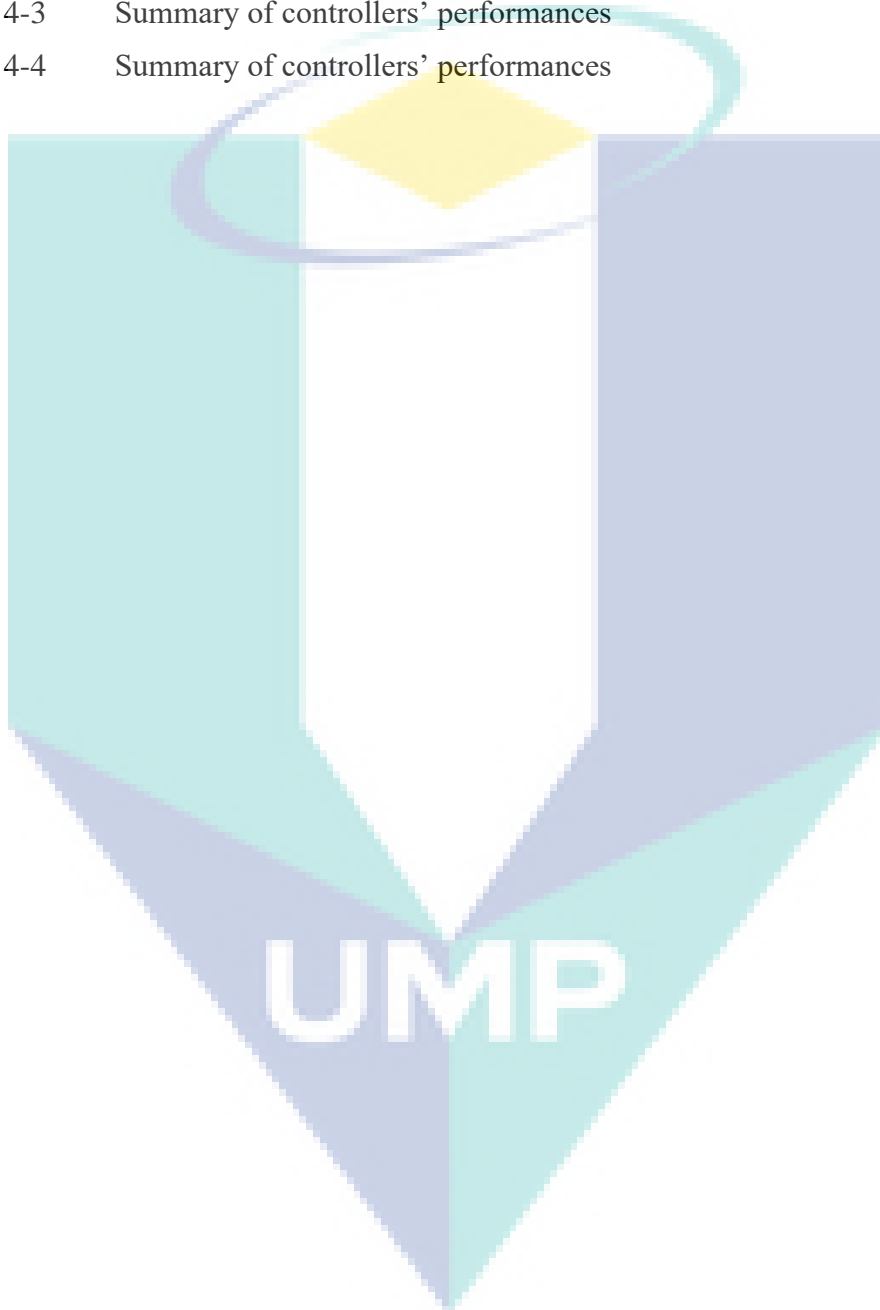
CHAPTER 3 METHODOLOGY	11
3.1 Introduction	11
3.2 Nonlinear model of AUG for longitudinal plane	11
3.3 Model linearisation	16
3.4 Controller design	19
3.4.1 Quasi Sliding Mode Control (QSMC)	19
3.4.2 Linear Quadratic Regulator (LQR)	21
3.5 Prototype development and system integration	22
3.5.1 Mechanical design and fabrication	22
3.5.2 Internal Frame	23
3.5.3 Ballast tank	24
3.5.4 Internal movable sliding mass	25
3.6 Electronic components and system integration	26
3.6.1 Controller module	26
3.6.2 Sensor module	29
3.6.3 Internal Actuator module	30
3.6.4 Communication module	31
3.6.5 Data logger module	32
CHAPTER 4 RESULTS AND DISCUSSION	33
4.1 Introduction	33
4.2 Performance of sliding mode control	33
4.3 Prototype testing and experimental	40
4.3.1 Water proof and buoyancy test	40
4.3.2 Functionality and reliability test	42

CHAPTER 5 CONCLUSION	47
5.1 Conclusion	47
5.2 Recommendation	47
REFERENCES	49
LIST OF PUBLICATIONS	52



LIST OF TABLES

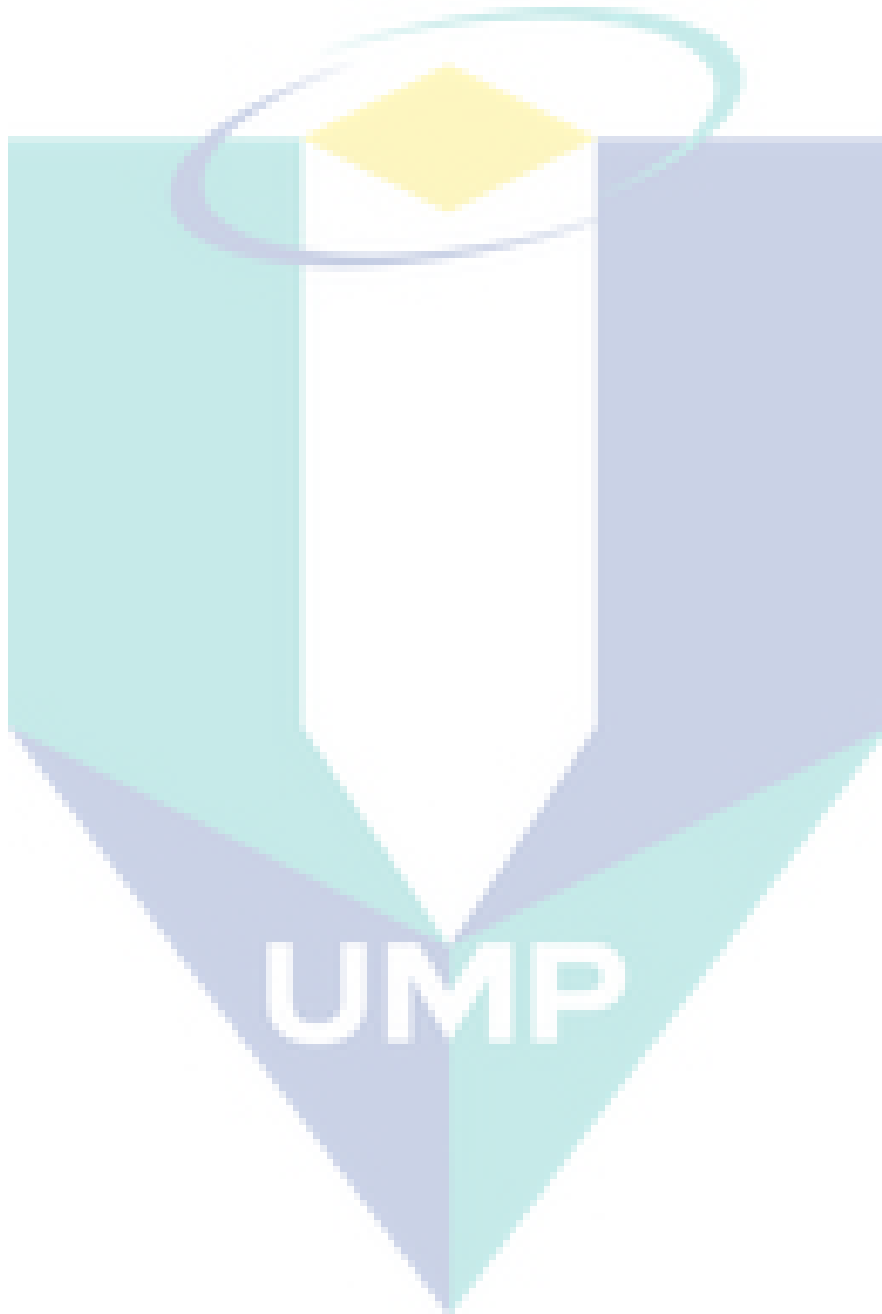
Table 3-1	The notations of the AUG	12
Table 4-1	Parameter values of the AUG	33
Table 4-2	The initial and desired values of the states	34
Table 4-3	Summary of controllers' performances	40
Table 4-4	Summary of controllers' performances	46



LIST OF FIGURES

Figure 1-1	The classification of underwater vehicles (Md Zain, 2012)	1
Figure 1-2	Gliding motion of AUG (Isa, 2015)	2
Figure 3-1	The reference frame of the glider	12
Figure 3-2	The simplified internal masses of the glider (Graver, 2005)	13
Figure 3-3	The flow of Quasi SMC design	20
Figure 3-4	Final prototype of the autonomous underwater glider	23
Figure 3-5	Internal frame of the AUG	24
Figure 3-6	Ballast tank installation and configuration	25
Figure 3-7	Internal movable mass installation	25
Figure 3-8	Bottom view of the internal sliding mass (a) Linear motor and (b) Threaded	26
Figure 3-9	Controller module	27
Figure 3-10	MATLAB™ to communicate with the Arduino through serial	28
Figure 3-11	Arduino code to read from MATLAB™.	28
Figure 3-12	IMU and compass	29
Figure 3-13	Ballast pump control circuit	31
Figure 3-14	Linear actuator control circuit	31
Figure 3-15	The DS-XTend RF module	32
Figure 3-16	SD card data logger	32
Figure 4-1	The block diagram of a QSMC	34
Figure 4-2	Gliding angle, ξ (downward glide)	36
Figure 4-3	Pitching angle, θ (downward glide)	36
Figure 4-4	Horizontal velocity, v_1 (downward glide)	37
Figure 4-5	Vertical velocity, v_3 (downward glide)	37
Figure 4-6	Gliding angle, ξ (upward glide)	38
Figure 4-7	Pitching angle, θ (downward glide)	38
Figure 4-8	Horizontal velocity, v_1 (upward glide)	39
Figure 4-9	Vertical velocity, v_3 (upward glide)	39
Figure 4-10	Waterproof and buoyancy test: (a) test without wings and tail wings inside water tank, (b) test with wings, (c) test with tail wings, (d) test with complete glider.	41
Figure 4-11	Compass module reliability test	42
Figure 4-12	IMU reliability test of the roll angle	43
Figure 4-13	IMU reliability test of the pitch angle	43

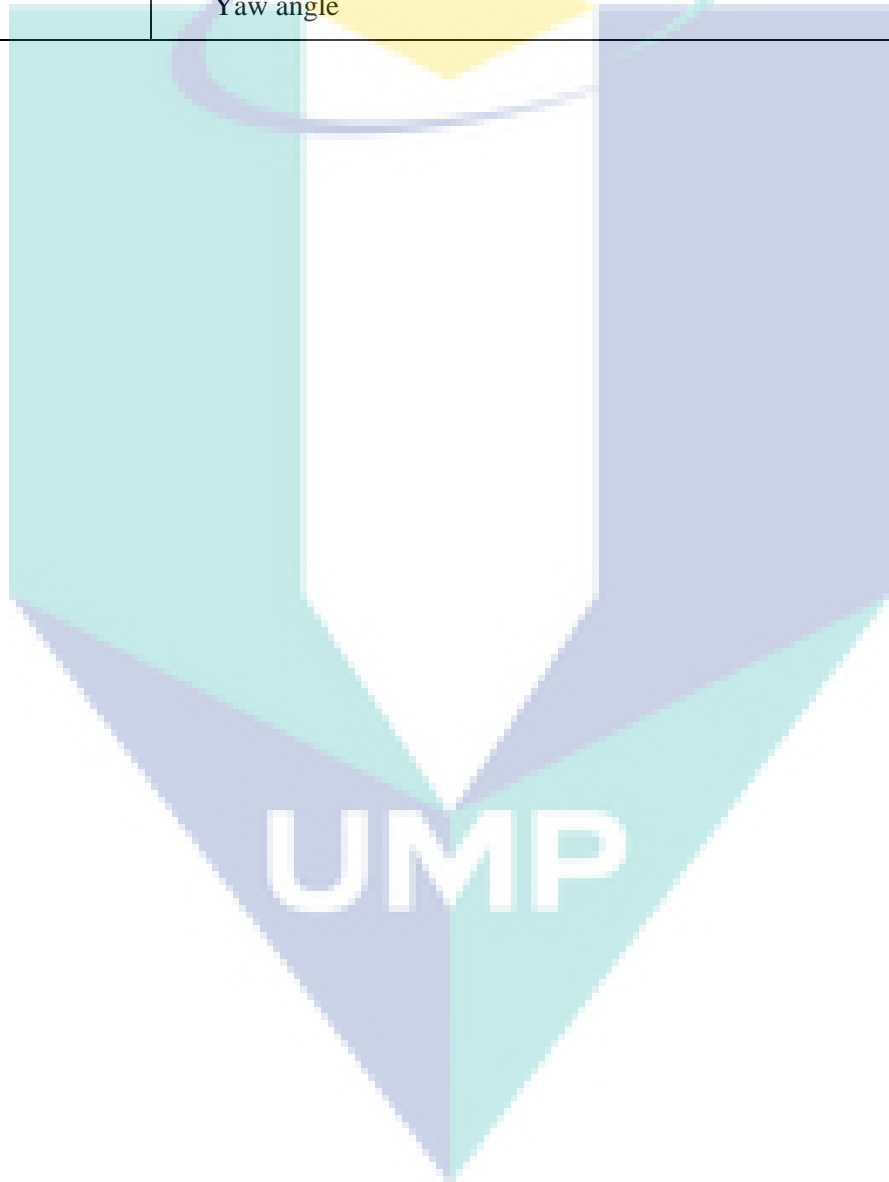
Figure 4-14	Transmitted GPS data	44
Figure 4-15	Threaded rod of the ballast pump	45
Figure 4-16	The motion of the internal sliding mass: (a) initial position, (b) Maximum position	45



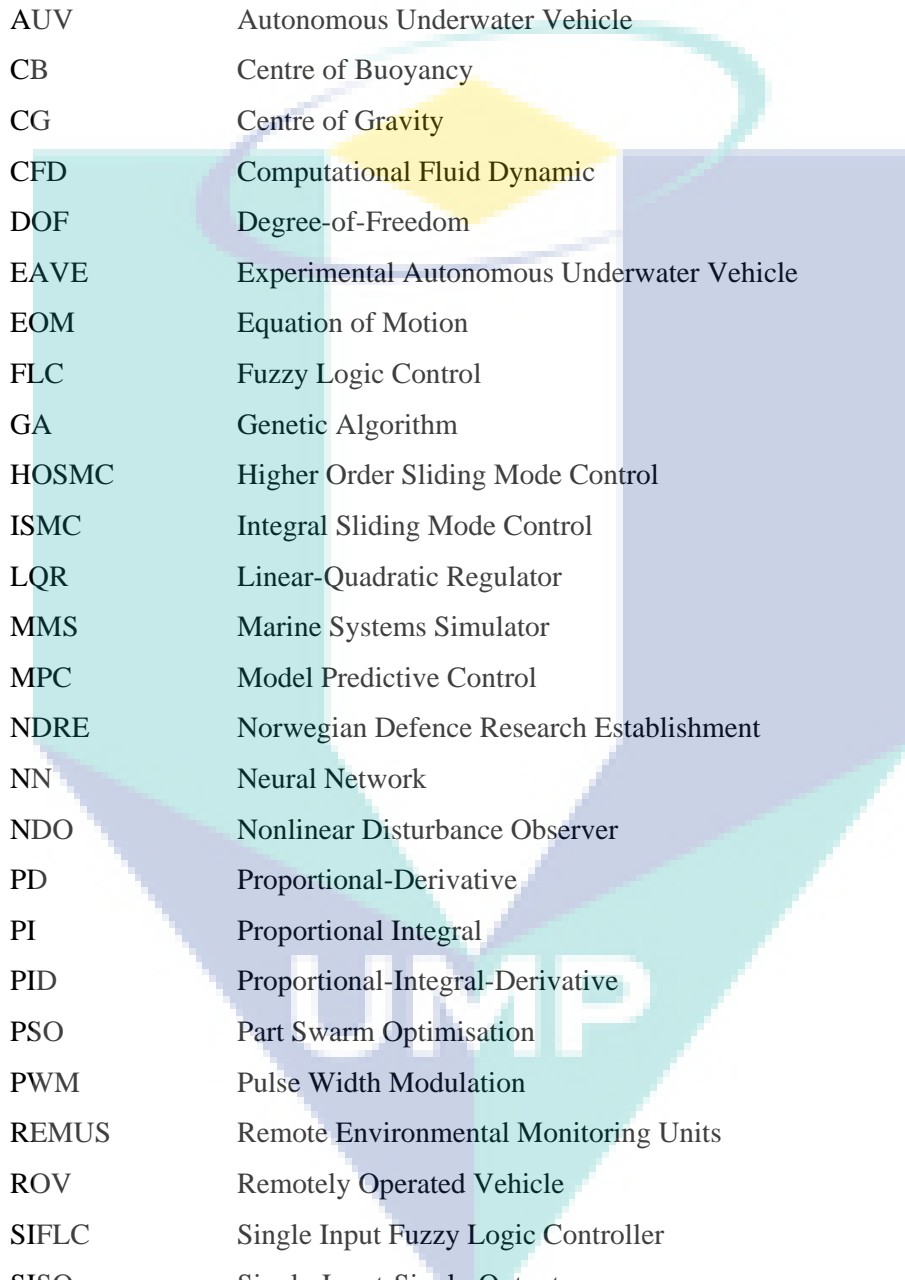
LIST OF SYMBOLS

α	Angle of attack
m_b	Ballast point mass
u_b	Ballast pumping rate
D	Drag
C_D, C_{D0}	Drag coefficients
m_{em}	Excess mass (net buoyancy) of AUG
m_w	Fixed point mass
g	Gravitational acceleration
v_3	Heave
m_h	Hull mass
J_1, J_2, J_3	Inertia of AUG
m_i	i^{th} diagonal element of total mass
u_i	i^{th} control law for BSTSMC
u_{i1}	i^{th} discontinuous control law for BSTSMC
s_i	i^{th} sliding surface
δ_k	k^{th} bounded matched perturbation
e_k	k^{th} tracking error
ρ_k	k^{th} upper bounded matched perturbation
$K_{\omega_2^1}, K_{\omega_2^2}$	Linear and nonlinear quadratic damping constant coefficients
m_p	Internal moving mass of AUG
L	Lift
C_L, C_{L0}	Lift coefficients
C_M, C_{M0}	Moment coefficients
w_{10}, w_{20}	Nominal control law for BISTSMC application in AUG
ω_2	Pitch rate (AUG)
θ	Pitching angle
M_{DL2}	Pitching moment
ω_1	Roll angle
R	Rotation matrix
α_1	Stabilising function for BSTSMC
β	Sideslip angle
P_p	Momentum of internal movable mass

P_{p1}	Momentum of internal movable mass in x-axis
P_{p3}	Momentum of internal movable mass in z-axis
v_1	Surge
r_b	Vector of ballast point mass
r_p	Vector of internal movable mass
r_{p1}	Vector of internal movable in x-axis
r_{p3}	Vector internal movable mass in z-axis
ω_3	Yaw angle

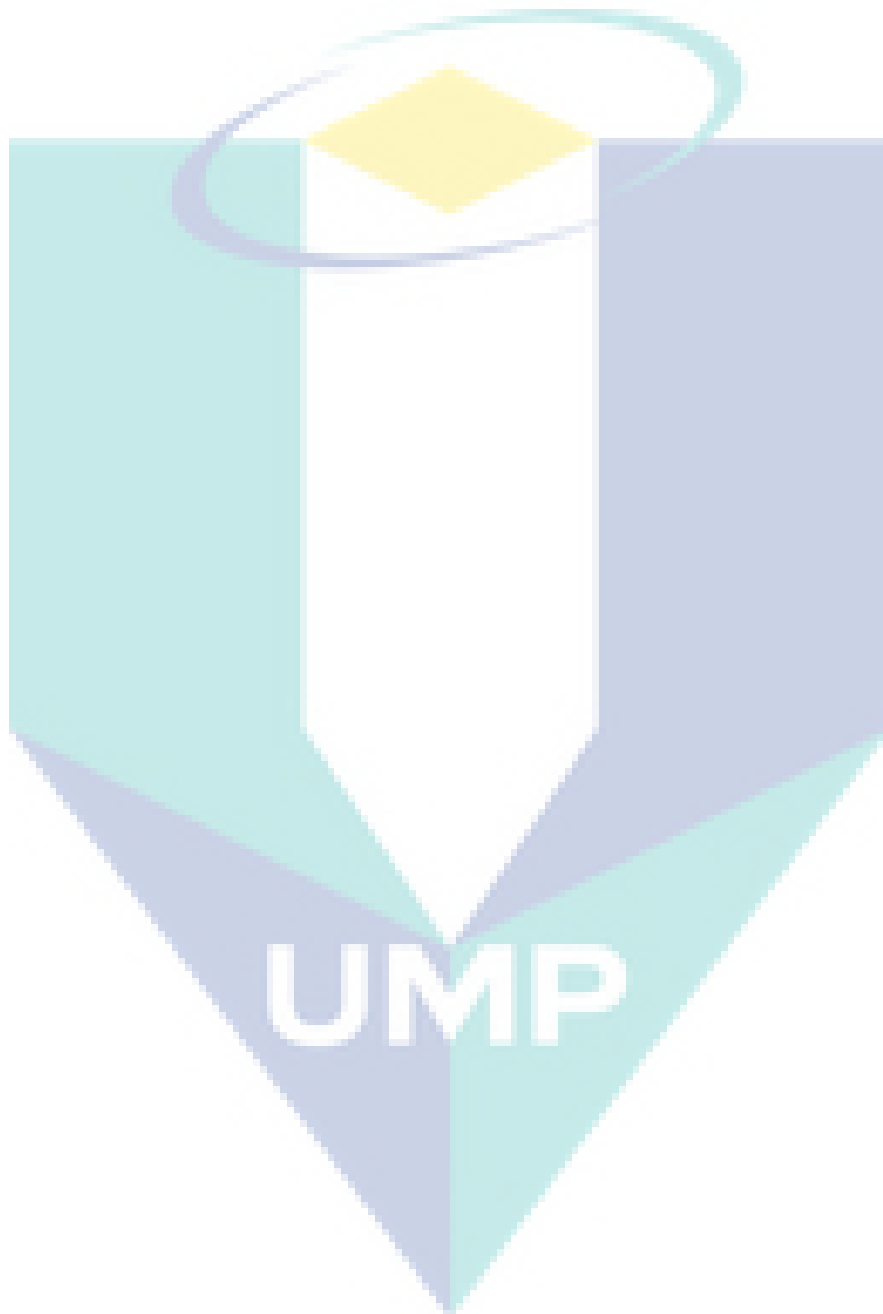


LIST OF ABBREVIATIONS



2D	Two-Dimensional
3D	Three-Dimensional
AUG	Autonomous Underwater Glider
AUV	Autonomous Underwater Vehicle
CB	Centre of Buoyancy
CG	Centre of Gravity
CFD	Computational Fluid Dynamic
DOF	Degree-of-Freedom
EAVE	Experimental Autonomous Underwater Vehicle
EOM	Equation of Motion
FLC	Fuzzy Logic Control
GA	Genetic Algorithm
HOSMC	Higher Order Sliding Mode Control
ISMC	Integral Sliding Mode Control
LQR	Linear-Quadratic Regulator
MMS	Marine Systems Simulator
MPC	Model Predictive Control
NDRE	Norwegian Defence Research Establishment
NN	Neural Network
NDO	Nonlinear Disturbance Observer
PD	Proportional-Derivative
PI	Proportional Integral
PID	Proportional-Integral-Derivative
PSO	Part Swarm Optimisation
PWM	Pulse Width Modulation
REMUS	Remote Environmental Monitoring Units
ROV	Remotely Operated Vehicle
SIFLC	Single Input Fuzzy Logic Controller
SISO	Single-Input-Single-Output
SMC	Sliding Mode Control
SMCB	SMC based on boundary layer
SMCS	SMC based on saturation function
SONCS	Self-Organizing Neural-net Control System
SOSMC	Second Oeder Sliding Mode Control

SPURV	Self-Propelled Underwater Research Vehicle
UARS	Unmanned Arctic Research Submersible
UV	Underwater Vehicle
UUV	Unmanned Underwater Vehicle
WHOI	Woods Hole Oceanography Institute



CHAPTER 1

INTRODUCTION

1.1 Background

The underwater robotic researches have received great attention since the past three decades. The robotic technologies have helped the researchers in expanding the scientific underwater exploration such as scientific ocean exploration, surveillance, commercial inspection of undersea facilities and military operations. Generally, underwater vehicle (UV) is divided in two main categories which are manned and unmanned underwater vehicles (UUVs). The UUV is further divided into remote operated vehicles (ROVs) and autonomous underwater vehicles (AUVs). The classification of UVs is summarised in Figure 1-1. The autonomous underwater glider (AUG) is considered as a special class of AUVs.

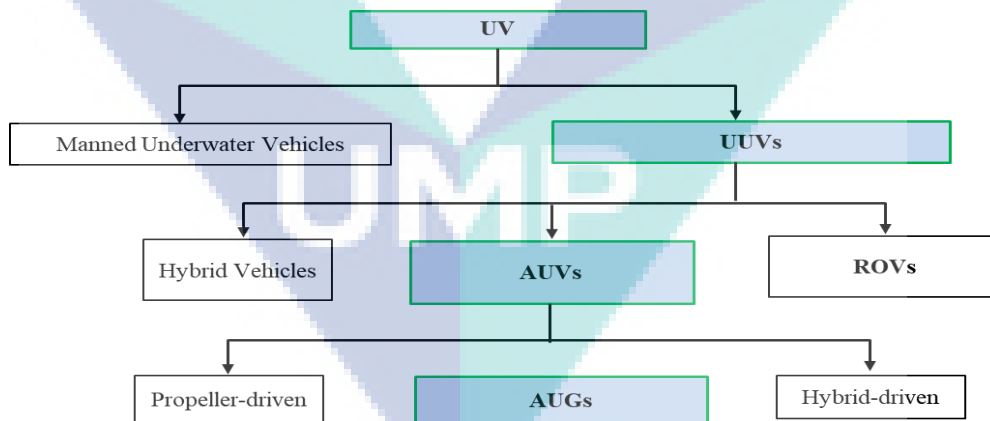


Figure 1-1 The classification of underwater vehicles (Md Zain, 2012)

The underwater glider was inspired by Henry Stommel (1989), called Slocum float. A decade later, three operational gliders namely Slocum (Webb et al., 2001),

Spray (Sherman et al., 2001) and Seaglider (Eriksen et al., 2001) were developed and tested, and their performance was proven.

The basic design of the AUG is buoyancy-driven with fixed wings and rudder, internal masses and a ballast pump. The AUG glides through the water column by shifting the internal movable mass in translational or rotational depending on the design of the movable tracks and pumping of the ballast pump. By doing these, the pitching angle and the depth can be controlled and cause the AUG to glide in saw-tooth pattern. Figure 1-2 shows the ideal gliding of a buoyancy-driven AUG.

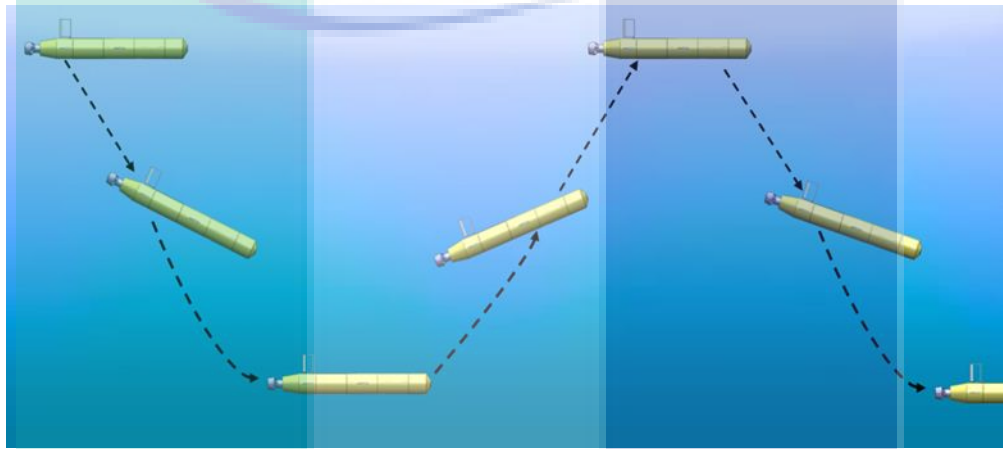


Figure 1-2 Gliding motion of AUG (Isa, 2015)

There are many control techniques either classical control or modern control have been employed to control AUVs and AUGs beginning from the simple proportional-integral-derivative (PID), linear-quadratic-regulator (LQR), robust control approach, adaptive control up to intelligent control such as fuzzy logic and neural network (NN). Among all the controllers, PID and LQR are widely used to control the existing gliders motion and attitude.

The sliding mode control (SMC) is one of the candidates that can be considered to improve the tracking performance of the parameters under study (control). Although the conventional SMC has suffered internally with chattering issues, however when the chattering phenomena is remedied, then the SMC is able to handle the parameter variation issue and offer the robustness towards external disturbances and uncertainties which are proven through many applications in many other systems (Jalani et al., 2010; Rhif, 2012; Li et al., 2013; Ismail et al., 2015). In this study the chattering phenomena is reduced through using of boundary layer SMC.

1.2 Problem Statement

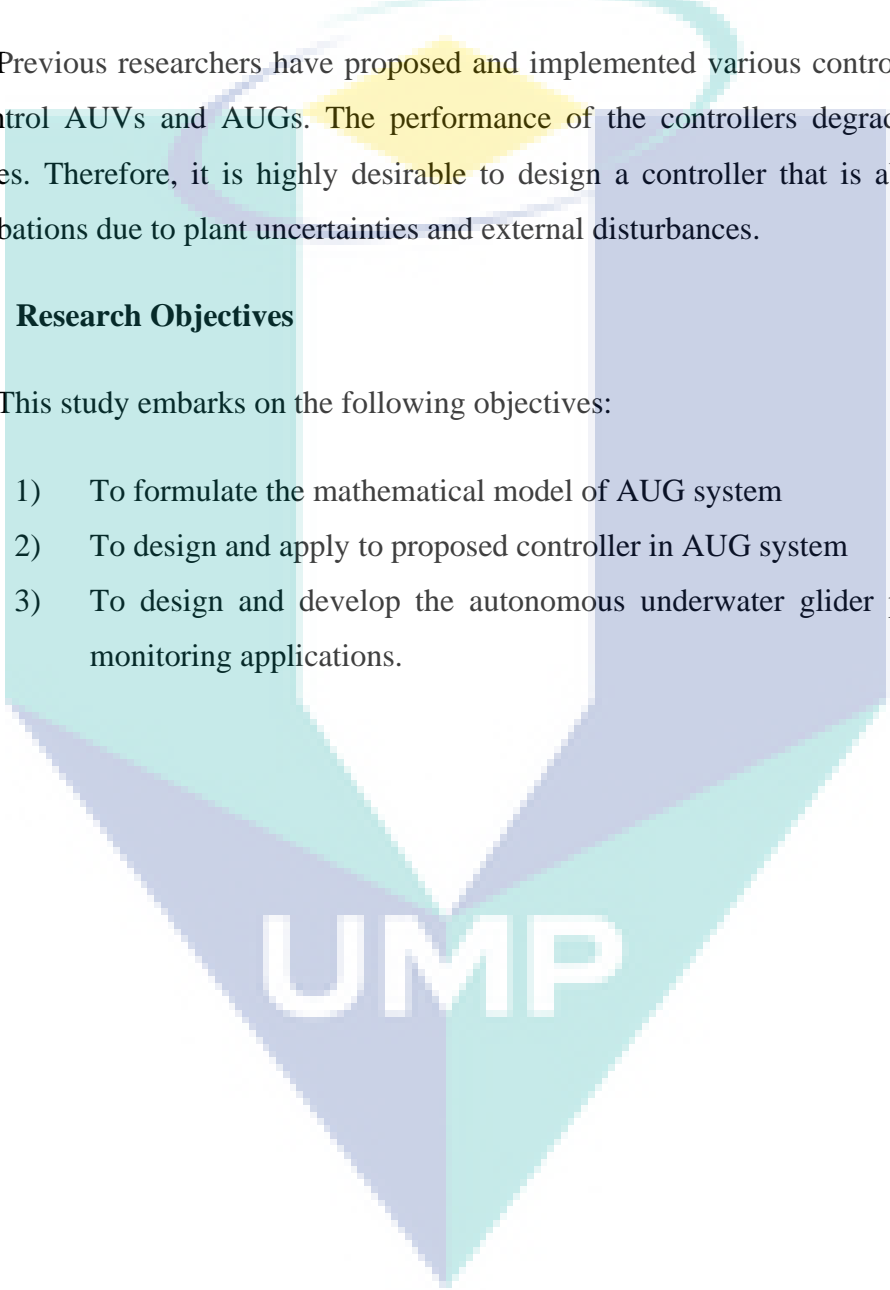
The AUG is considered as an under-actuated system with high nonlinearity of dynamics, with uncertainties in hydrodynamic coefficients and with the presence of underwater disturbance (J. Yuh, 2000; Pan & Xin, 2012). Therefore, a robust nonlinear controller algorithm is required to maintain the overall performance of the AUG.

Previous researchers have proposed and implemented various control techniques to control AUVs and AUGs. The performance of the controllers degrades with the changes. Therefore, it is highly desirable to design a controller that is able to reject perturbations due to plant uncertainties and external disturbances.

1.3 Research Objectives

This study embarks on the following objectives:

- 1) To formulate the mathematical model of AUG system
- 2) To design and apply to proposed controller in AUG system
- 3) To design and develop the autonomous underwater glider platform for monitoring applications.



UMP

CHAPTER 2

LITERATURE REVIEW

2.1 Introduction

For UVs to manoeuvre autonomously, the control algorithm must be robust against perturbations and parameter variations. It is known that the UVs are difficult to control since their system is highly nonlinear and the dynamics of the vehicles are time-varying. The hydrodynamics coefficients are uncertain, mostly disturbed by water current and also changes in centre of buoyancy (CB) and centre of gravity (CG) due to the internal actuators (Budiyono, 2009; Yuh, 2000). There have been various control techniques proposed to control the AUVs and AUGs. The control techniques to control the AUVs and AUGs are divided into three main categories; linear control, nonlinear control and intelligent control strategies. This section covers the literatures of SMC applications to cover wide spectrum of literatures.

2.2 Control Strategies

In order for the underwater vehicles to be autonomous, the vehicle control system must be robust and adaptive to the dynamics variation in its behaviour and environment. It is difficult to control underwater vehicles due to several constraints: the highly nonlinear and time-varying dynamics behaviour of the vehicle; uncertainties in hydrodynamics coefficients; disturbances by water currents; and changes of centre of buoyancy (CB) and centre of gravity (CG) due to the presence of internal actuators (Budiyono, 2009; Yuh, 2000). Various control methods have been proposed by researchers to control AUVs and AUGs, whether through simulation or actual experiment (Budiyono, 2009; Yuh, 2000).

2.2.1 Linear Control Strategies

Linear control is used when the model of the plant is linearised about the equilibrium. In underwater vehicle, the linear control is dominated by the proportional-integral-derivative (PID) and linear quadratic regulator (LQR).

The first implementation of PID in AUVs was proposed by Chellabi & Nahon (1993). Nonlinear dynamics of the AUV were linearised and decoupled into six SISO second-order subsystems. A combined strategy of a proportional-derivative (PD) controller and LQR was proposed for the six SISO subsystems. The PD control law was designed to stabilise the system and LQR was used to cater the optimal error correcting term for improving the robustness of the PD controller. Following this first implementation, Jalving (1994) proposed a PID controller for Norwegian Defence Research Establishment (NDRE) AUV. The nonlinear dynamics were linearised and decoupled into three subsystems which were speed, steering and diving subsystems. The speed subsystem was controlled using PI control law and this PD control law was utilised to control heading and depth. In the unmanned underwater test vehicle, Lee et al. (2009) proposed a PID controller for Manta-type unmanned underwater test vehicle to control steering and diving based on linearised model. In 2010, Santhakumar & Asokan (2010) proposed a self-tuning PID to enhance the performance of the original PID. In this work, Taguchi's method was used to build the self-tuning PID algorithm. Recently, the self-tuning performance was compared with tuning method proposed by Ziegler-Nichols. Other than these, in 2014, Watson & Green (2014) proposed a PID for micro AUV to control depth. The continuous PID was discretised using Tustin approximation to compute the discrete version of PID controller.

Leonard & Graver (2001) designed the LQR for the ROGUE AUG. The LQR was designed for steady glides of 30° and 45° downward and upward. There was no significant tuning performed to optimise the controller parameters. Joo & Qu (2015) designed LQR to control the motion of a hybrid AUV. The LQR performance was tested for steady glide of 30° downward and upward. In the same year, Javaid et al. (2015) designed the LQR to control the longitudinal plane of the AUG. The LQR was simulated for two different wing designs which were tapered shape and rectangular shape to observe the behaviour of the glider motion with different shape of wing.

Recently, Tchillian et al (2016) also proposed the LQR for the longitudinal plane of an AUG.

As conclusion, the linear controllers provide good tracking performances. However, since the model is linearised about the equilibrium point, the performance of the controller is only effective in a small neighbourhood of the equilibrium.

2.2.2 Nonlinear Control Strategies

Most of the systems are nonlinear. The nonlinear control strategies offer a better option in handling the nonlinearities, uncertainties, disturbances and changes in parameters in which linear control strategy is unable to handle. There are various nonlinear controls have been implemented in AUVs and AUGs such as SMC, back-stepping control and adaptive control.

The SMC strategy is known for its robustness against perturbations such as parameter variations and external disturbances. Since the UVs are highly nonlinear with time variant dynamics, thus it is found in many research works in which the SMC technique was employed. The main drawback of the SMC is chattering phenomena that is induced by high frequency switching of the discontinuous control. However, many approaches can be used to reduce the chattering phenomena.

The first implementation of SMC in AUVs was found in 1985 by Yoerger & Slotine (1985). In this research, the boundary layer SMC control law was developed for the Experimental Autonomous Vehicle (EAVE) and this control law was only developed for the nonlinear model for the horizontal plane. Dougherty et al. (1988) proposed the conventional SMC that employed the signum function in discontinuous control. The controller was designed for hovering control of an AUV. Later, Healey & Lienard (1993) implemented SMC to control speed, heading and depth. The controller was designed based on decoupled subsystems which were speed, steering and diving subsystems. They employed the hyperbolic tangent smooth function to replace the

signum function. Wang et al. (2002) employed the basic SMC which its signum function was employed in the discontinuous control for 5 DOF nonlinear system that controlled surge, sway, heave, pitching and yaw of a ZHISHUI-III AUV. In 2015, Kim et al. (2015) employed integral sliding mode control ISMC to reduce chattering. ISMC is also known as no reaching phase SMC until now since the algorithm ensures that the sliding begins at time, $t = 0$. In addition, Kim et al. (2015) had also developed controller control depth of Cyclops AUV.

The back-stepping is another technique used to control the motion of the AUVs and AUGs. The back-stepping is known as a recursive systematic design methodology. It uses Lyapunov stability theorem to analyse the stability of the controller. The basic idea of back-stepping is the design that breaks up into sequence of the sub-problems of the lower order of the system and then recursively uses the states as “virtual controls” to attain the intermediate control laws using the Lyapunov function.

Caiti & Calabro (2010) proposed the integral back-stepping technique with fuzzy to improve the adaptation of the controller to hydrodynamics uncertainties and external disturbances. The controller was designed for the FOLAGA AUV. Ferreira et al (2011) proposed the back-stepping control to the MARES AUV in the presence of thruster fault. Two control laws were derived to control the pitching angle and the depth of MARES AUV. Wei et al. (2015) researched on the back-stepping control based on nonlinear disturbance observer (NDO) to control the depth of the AUV. The NDO is commonly used to estimate the disturbance. In Cervantes et al (2016), the output based back-stepping was proposed to control the linear position and yaw angle of the AUV. The algorithm of this work combined the back-stepping like form and a robust exact differentiator. The simulation results proved that the proposed controller provided an acceptable performance. For AUG, several works based on back-stepping control were reported in (Burlion et al., , 2004; Caiti et al., 2012; Cao et al., 2015; Cao et al, 2016).

In Antonelli et al. (2001), the adaptive control was designed to control the six degree of freedom (DOF) of ODIN ROV and AUV that combined SMC with an adaptive controller system parameter estimation. Later, Antonelli (2007) presented the

adaptive control to control 6 DOFs of ODIN and AUV. However, in this work, the adaptive controller was a combination of PD with an adaptive/integral compensator to compensate the persistent dynamic effects such as the restoring forces and the ocean currents. In 2014, Sahu & Subudhi (2014) designed the adaptive controller to control the liner position and yaw angle of AUV. The adaptive control was combined with PD controller which was able to adapt the uncertainties in hydrodynamic parameters. One year later, Barbalata et al. (2015) proposed the adaptive control method to control the 4 DOFs of AUV. The adaptive control was used to determine the gain of the PD controller online basis through position/velocity error.

In general, the nonlinear control provides high robustness against nonlinear dynamics, uncertainties in hydrodynamic and environment disturbances.

2.2.3 Intelligent Control Strategies

There are several categories of control algorithms fall under intelligent control. The NN and fuzzy logic controls (FLCs) are the most prominent controls employed for controlling the motion of the underwater vehicles. The advantage of intelligent control is its ability to adapt and robustness to the nature of highly nonlinear and dynamic environment of the underwater vehicles.

Various researches have been done previously using NN as a backbone to control the AUVs. In 2010, Amin et al. (2010) introduced two online learning methods which were an online multilayer perceptron NN (OMLPNN) and online recurrent multilayer perceptron NN (ORMLPNN) to control a testbed NPS AUV. The controllers were designed to compute the forces and moments of the AUV so that the tracking error could be eliminated and the inverse model of AUV could be generated in which also determined the speed of the propeller angles of control surface. García-Córdova and Guerrero-González (2011) proposed a biologically-inspired NN for trajectory tracking of AUVs. The Self-Organisation Direction Mapping Network (SODMN) which was an unsupervised kinematic adaptive NN controller was designed for guiding an AUV towards a target in a 3D workspace. The angular velocity of each propeller was selected in order to control the motion of the AUV. The AUV motions were controlled by selecting the angular velocity of each propeller. Eski & Yildirim (2014) designed robust controller based on NN for linear model of AUV. The NN was designed based on

resilient back-propagation structure to adjust the weights of the NN. The performance of the proposed control was compared to the PID controller.

The ability of FLC to approximate the nonlinear mapping of the system from input to output, makes it suitable for nonlinear control (Zhao & Yuh, 2005). The satisfactory performance of the FLC can be achieved by defining the correct fuzzification and membership functions. Nevertheless, the experimental data is needed for defining the correct fuzzification of the membership functions and fuzzy rules and thus increasing the computational time. Ishaque et al. (2010) and Amjad et al. (2010) proposed a Single Input Fuzzy Logic Controller (SIFLC). This controller was simulated using Marine System Simulator (MSS). It has reduced tuning effort and computational time in the orders of two magnitudes than the conventional FLC. The FLC type Sugeno model was proposed by Lee & Kang (1998). It was implemented in underwater vehicle by taking into account the influence thruster dynamic. In terms of system algorithm, the research made by Gua & Huang (1996) proposed an algorithm that combined the genetic algorithm (GA) and FLC to control the AUVs. The GA was used to optimise the membership function. The fitness functions were designed such that the rise time, maximum overshoot and steady state error are satisfied.

In general, the intelligent control offers very good tracking performance and adaptability to hydrodynamics uncertainties and environmental disturbances. However, it usually suffers from the computational time during the tuning process and the parameter estimation process (Zhao & Yuh, 2005).

2.3 Autonomous Underwater Glider Designs and Characteristics

This section discusses the designs and features of the existing AUGs, which group includes the hybrid-driven AUGs. The objective of this discussion is to guide the design of the hybrid-driven AUG so that the mathematical model, controller algorithm and prototype development of the glider could be developed.

The gliding flight of existing underwater gliders such as Slocum, Spray and Seaglider is buoyancy-driven, which means that they do not use thrusters or propellers. They have a cylindrical or ellipsoidal hull with nose and tail, wings, a rudder, a ballast pump, internal moving masses, and batteries as a power system. Internal electronic

components include the sensors, microcontroller, communication module and data logger.

In order to travel in a zigzag pattern through the ocean, these vehicles change depth and pitch to glide. The depth is varied by continuously controlling their buoyancy level from neutrally buoyant to negatively and positively buoyant using a ballast pump, and the pitch is changed by controlling their internal moving mass. Conventionally, existing gliders have fixed wings, and they control their attitude (such as roll and pitch) by moving their internal masses and a rudder (Graver, 2005). They are relatively slow-moving due to conserved power, so that they could be used for long-duration missions. Their maximum speeds are 0.5 knot, and most of the power is used for ballast pumping (Jenkins et al., 2003).

In this work, there are 14 AUGs that have been reviewed in terms of mechanical and electronic designs and characteristics as well as control mechanisms and performance characteristics. These AUGs are: Slocum Battery and Slocum Thermal (Bender et al., 2008; Graver, 2005; Griffiths et al., 2002; Rudnick et al., 2004; Webb et al., 2001; Wood, 2009), Spray (Bender et al., 2008; Graver, 2005; Griffiths et al., 2002; Rudnick et al., 2004; Sherman et al., 2001; Wood, 2009), Seaglider (Bender et al., 2008; Eriksen et al., 2001; Griffiths et al., 2002; Rudnick et al., 2004; Wood, 2009), Deepglider (Osse and Eriksen, 2007; Wood, 2009), ALBAC (Graver, 2005; Kawaguchi et al., 1993; Wood, 2009), Liberdade XRAY (ONR, 2006; Wood, 2009), ROGUE (Graver and Leonard, 2001; Graver, 2005; Leonard and Graver, 2001; Mahmoudian, 2009), STERNE (Graver, 2005; Griffiths et al., 2007; Hussain et al., 2011; Moitie and Seube, 2001; Wood, 2009), ALEX (Arima et al., 2008, 2009; Ichihashi et al., 2008), Folaga (Alvarez et al., 2009; Caffaz et al., 2010), PETREL (Wang et al., 2010, 2011), Tsukuyomi (Asakawa et al., 2011, 2012), and Hybrid glider (Peng et al., 2013).

CHAPTER 3

METHODOLOGY

3.1 Introduction

This chapter presents the modelling of the AUG system, design of control algorithm and prototype development and integration. The process of establishing the nonlinear model is explained in Section 3.2. Then using the nonlinear model to obtain the linearised model will be explained in Section 3.3. The controller for the linearised system designed based on the SMC is explained in Section 3.4.1. The performance of the proposed is compared to the performance of the linear quadratic regulator (LQR) where the design of LQR is explained in Section 3.4.2. Finally, prototype development and integration is explained in Section 3.5.

3.2 Nonlinear model of AUG for longitudinal plane

The mathematical model of the longitudinal plane of AUG is based on the model proposed by Graver (2005). The model was proposed with the assumption that the internal movable mass moves along the x and z axes. Two reference frames of the glider are defined, and the initial frame (i-frame) and the body frame (b-frame) are shown in Figure 3-1. The initial frame is assumed to be non-rotating (fixed) frame. The body frame is fixed to the glider's body with its origin at CB. The body axes are specified as X , Y , and Z which lay along the x -axis, y -axis, and z -axis respectively. The notations of the overall AUG model are specified in **Error! Reference source not found.** The CG is assumed to coincide with CB.

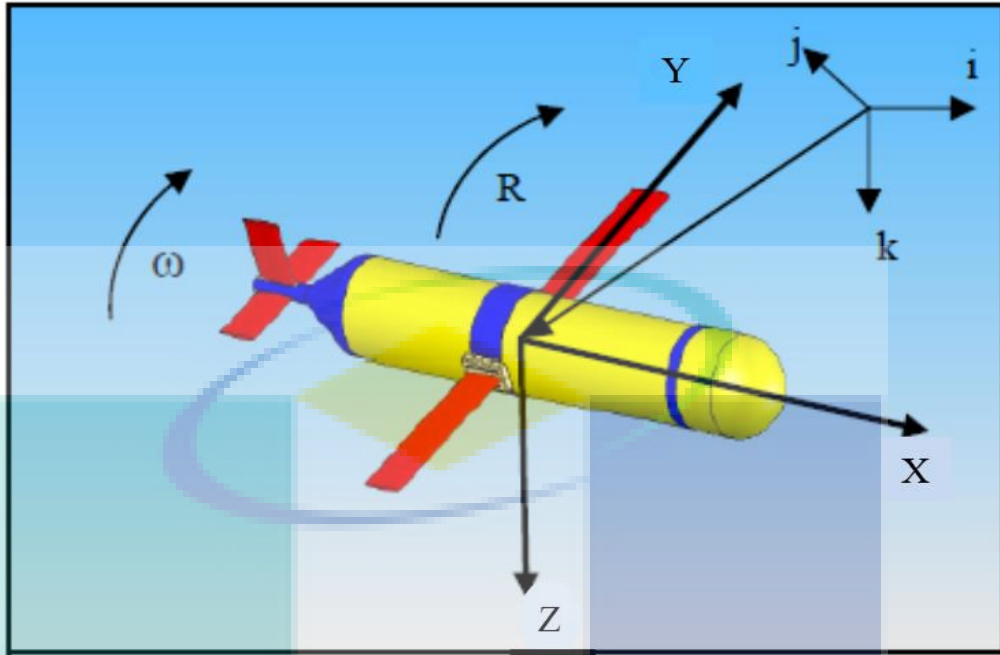


Figure 3-1 The reference frame of the glider

Table 3-1 The notations of the AUG

	Linear and angular velocity	Position and orientation
Motion in the x-direction (surge)	v_1 (m/s)	x
Motion in the y-direction (sway)	v_2 (m/s)	y
Motion in the z-direction (heave)	v_3 (m/s)	z
Rotation about the x-axis (roll)	ω_1 (rad/s)	ϕ
Rotation about the y-axis (pitching)	ω_2 (rad/s)	θ
Rotation about the z-axis (yaw)	ω_3 (rad/s)	ψ

The longitudinal model based on Graver (2005) is presented in this sub-chapter. The detail derivation of Graver's work can be found in Graver et al. (1998) and Leonard & Graver (2001). The following assumptions have been made to reduce the complexity of the model without jeopardising the overall performance of the glider.

- i) The offset static mass, m_w was set to zero ($m_w = 0$)

- ii) The ballast point mass was fixed at the centroid of the glider body ($r_b = 0$).

The assumptions have caused the glider to be in its simplified internal masses as shown in Figure 3-2. The assumptions also eliminated the coupling due to offset static mass, and the coupling between the ballast and the glider inertia and the pitching moment.

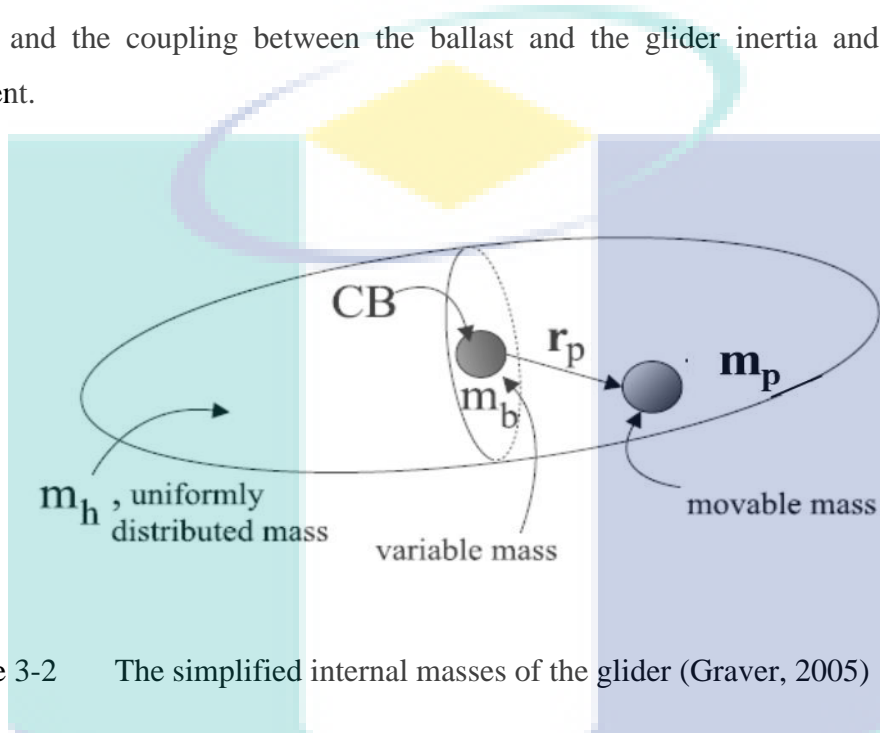


Figure 3-2 The simplified internal masses of the glider (Graver, 2005)

The longitudinal plane model was established by setting all the parameters related to lateral to zero, lateral position (y), lateral velocity (v_2), roll rate (ω_1) and yaw rate (ω_3) as shown in the matrices form below.

Rotation matrix:

$$R = \begin{bmatrix} \cos\theta & 0 & \sin\theta \\ 0 & 1 & 0 \\ -\sin\theta & 0 & \cos\theta \end{bmatrix} \quad 3-1$$

Body position:

$$b = \begin{bmatrix} x \\ 0 \\ z \end{bmatrix} \quad 3-2$$

Linear velocity:

$$\mathbf{v} = \begin{bmatrix} v_1 \\ 0 \\ v_3 \end{bmatrix} \quad 3-3$$

Angular velocity:

$$\boldsymbol{\omega} = \begin{bmatrix} 0 \\ \omega_2 \\ 0 \end{bmatrix} \quad 3-4$$

Internal movable position:

$$\mathbf{r}_p = \begin{bmatrix} r_{p1} \\ 0 \\ r_{p3} \end{bmatrix} \quad 3-5$$

Internal movable mass momentum:

$$\mathbf{P}_p = \begin{bmatrix} P_{p1} \\ 0 \\ P_{p3} \end{bmatrix} \quad 3-6$$

Control input:

$$\mathbf{u} = \begin{bmatrix} u_{aug1} \\ 0 \\ u_{aug3} \end{bmatrix} \quad 3-7$$

The above setup has produced the equation of motion (EOM) for the longitudinal plane as written in Equation (3-8) – (3-18).

$$\dot{x} = v_1 \cos(\theta) + v_3 \sin(\theta) \quad 3-8$$

$$\dot{z} = -v_1 \sin(\theta) + v_3 \cos(\theta) \quad 3-9$$

$$\dot{\theta} = \omega_2 \quad 3-10$$

$$\begin{aligned} \dot{\omega}_2 = \frac{1}{J_2} \{ & (m_3 - m_1)v_1v_3 - (r_{p1}P_{p1}\omega_2 + r_{p3}P_{p3})\omega_2 \\ & - m_p g(r_{p1} \cos(\theta) + r_{p3} \sin(\theta)) + M_{DL2} - r_{p3}u_{aug1} \\ & + r_{p1}u_{aug3} \} \end{aligned} \quad 3-11$$

$$\dot{v}_1 = \frac{1}{m_1} \{ -m_3v_3\omega_2 - P_{p3}\omega_2 - m_{em}g\sin(\theta) + L\sin(\alpha) - D\cos(\alpha) - u_{aug1} \} \quad 3-12$$

$$\dot{v}_3 = \frac{1}{m_3} \{ m_1v_1\omega_2 + P_{p1}\omega_2 + m_{em}g\cos(\theta) - L\cos(\alpha) - D\sin(\alpha) - u_{aug3} \} \quad 3-13$$

$$\dot{r}_{p1} = \frac{1}{m_p} P_{p1} - v_1 - r_{p3}\omega_2 \quad 3-14$$

$$\dot{r}_{p3} = \frac{1}{m_p} P_{p3} - v_3 + r_{p1}\omega_2 \quad 3-15$$

$$\dot{P}_{p1} = u_{aug1} \quad 3-16$$

$$\dot{P}_{p3} = u_{aug3} \quad 3-17$$

$$\dot{m}_b = u_b \quad 3-18$$

where m_{em} is the net buoyancy, m_1 , and m_3 denote the first and third element of total mass, D and L , and M_{DL2} represents the drag, lift and pitching moment of the hydrodynamic force and moment. They were defined by Graver (2005) as

$$m_{em} = m_h + m_p + m_b - m_{df} \quad 3-19$$

$$L = (C_{LO} + C_L\alpha)(v_1^2 + v_3^2) \quad 3-20$$

$$D = (C_{DO} + C_D\alpha^2)(v_1^2 + v_3^2) \quad 3-21$$

$$M_{DL2} = (C_{MO} + C_M\alpha)(v_1^2 + v_3^2) + K_{\omega_1}\omega_2 + K_{\omega_2}\omega_2^2 \quad 3-22$$

where m_h , m_p , and m_{df} are the mass of the hull, internal movable mass and displaced fluid mass respectively. α is the angle of attack. C_L , C_{LO} , C_D , C_{DO} , C_M , and C_{MO} are the hydrodynamic lift, drag and pitching moment coefficients respectively. The system and input states are defined as

$$\begin{aligned} x &= [x_1 \ x_2 \ x_3 \ x_4 \ x_5 \ x_6 \ x_7 \ x_8 \ x_9 \ x_{10}]^T \\ &= [z' \ \theta \ \omega_2 \ v_1 \ v_3 \ r_{p1} \ r_{p3} \ P_{p1} \ P_{p3} \ m_b]^T \end{aligned} \quad 3-23$$

$$u = [u_1 \ u_2 \ u_3]^T \quad 3-24$$

3.3 Model linearisation

The linearisation is performed around the gliding equilibrium as defined by Graver in (Joshua Grady Graver, 2005). In Taylor's series expansion method, the approximated of the nonlinear is performed by computing the gradient of the nonlinear equation with respect to each system state vector and input vector to obtain the system matrix A and input matrix B respectively. Consider the nonlinear system in Equation 3-25.

$$\dot{x}(t) = f(x(t), u(t)) \quad 3-25$$

where $f: \mathfrak{R}^n \times \mathfrak{R}^m \rightarrow \mathfrak{R}^n$ is the nonlinear function, $x(t) \in \mathfrak{R}^n$ and $u(t) \in \mathfrak{R}^m$ are the state vector and the input vector respectively. Using TSE the Equation 3-26 can be written as

$$\begin{aligned} \dot{x}(t) &= f(x_e, u_e) + \left. \frac{\partial f}{\partial x} \right|_{x=x_e} (x - x_e) + \left. \frac{\partial f}{\partial u} \right|_{x_e, u_e} (u - u_e) + \\ &\frac{1}{2} \left. \frac{\partial^2 f}{\partial x^2} \right|_{x_e, u_e} (x - x_e)^2 + \left. \frac{\partial^2 f}{\partial x \partial u} \right|_{x_e, u_e} (x - x_e)(u - u_e) + \frac{1}{2} \left. \frac{\partial^2 f}{\partial u^2} \right|_{x_e, u_e} (u - u_e)^2 + \end{aligned} \quad 3-26$$

higher order terms

where x_e , and u_e are the equilibrium points and equilibrium input points such that $f(x_e, u_e) = 0_n$. The Equation 3-26 can be simplified by taking only the first order term and neglecting all higher order terms. Yields Equation 3-27.

$$\dot{x}(t) \approx \left. \frac{\partial f}{\partial x} \right|_{x_e, u_e} (x - x_e) + \left. \frac{\partial f}{\partial u} \right|_{x_e, u_e} (u - u_e) \quad 3-27$$

Define the deviation variable, $\delta x = x - x_e$, and $\delta u = u - u_e$

$$\dot{\delta x} \approx \left. \frac{\partial f}{\partial x} \right|_{x_e, u_e} \delta x + \left. \frac{\partial f}{\partial u} \right|_{x_e, u_e} \delta u \quad 3-28$$

In a matrix form can be written as

$$\dot{\delta x} = A\delta x + B\delta u \quad 3-29$$

where system matrix, $A = \left. \frac{\partial f}{\partial x} \right|_{x_e, u_e} \in \mathfrak{R}^{n \times n}$, and input matrix, $B = \left. \frac{\partial f}{\partial u} \right|_{x_e, u_e} \in \mathfrak{R}^{m \times n}$

For linearised system, Equation 3-29 reformulated into a general uncertain linear time invariant (LTI) system as written in Equation 3-30

$$\dot{x} = A\delta x(t) + B\delta u(t) + Bh(x, t) \quad 3-30$$

Where $\delta x = x - x_d$, $\delta u = u - u_d$, $A \in R^{n \times n}$, and $B \in R^{n \times m}$, are the state vector, input vector, system matrix, and input matrix. $x \in R^n$ and $u \in R^m$, that satisfies the following assumptions:

1. Matrix B has a full rank (i.e. $rank(B) = m$), where $1 \leq m < n$
2. The pair (A, B) is controllable.
3. $h(x, t)$ is assumed known and in the range of input distribution B. $h(x, t)$ is a bounded matched perturbation that is a bounded with a known upper bound as defined in Equation (3-33)

$$|h(x, t)| \leq |d| \quad 3-31$$

The linearization is made for the steady gliding path of 30° downward and upward. The matrix A and B downward and upward glides are defined in Equations 3-32 and 3-33 respectively.

$$A_d = \begin{bmatrix} 0 & -0.30 & 0 & -0.11 & 0.99 & 0 & 0 & 0 & 0 & 0 \\ 0 & 0 & 1.00 & 0 & 0 & 0 & 0 & 0 & 0 & 0 \\ 0 & -0.83 & 0 & 0.12 & -44.37 & -19.83 & 8.70 & 0 & 0 & 0 \\ 0 & 6.40 & -0.03 & -0.18 & 0.10 & 0 & 0 & 0 & 0 & 0.13 \\ 0 & -2.88 & 0.31 & -0.61 & -2.91 & 0 & 0 & 0 & 0 & 0.51 \\ 0 & 0 & -0.04 & -1.00 & 0 & 0 & 0 & 1.20 & 0 & 0 \\ 0 & 0 & 0.004 & 0 & -1.00 & 0 & 0 & 0 & 1.20 & 0 \\ 0 & 0 & 0 & 0 & 0 & 0 & 0 & 0 & 0 & 0 \\ 0 & 0 & 0 & 0 & 0 & 0 & 0 & 0 & 0 & 0 \\ 0 & 0 & 0 & 0 & 0 & 0 & 0 & 0 & 0 & 0 \end{bmatrix} \quad 3-32$$

$$B_d = \begin{bmatrix} 0 & 0 & 0 \\ 0 & 0 & 0 \\ -0.11 & 0.01 & 0 \\ 0.03 & 0 & 0 \\ 0 & -0.03 & 0 \\ 0 & 0 & 0 \\ 0 & 0 & 0 \\ 1.00 & 0 & 0 \\ 0 & 1.00 & 0 \\ 0 & 0 & 1.00 \end{bmatrix}$$

$$A_u = \begin{bmatrix} 0 & -0.30 & 0 & -0.11 & 0.99 & 0 & 0 & 0 & 0 & 0 \\ 0 & 0 & 1.00 & 0 & 0 & 0 & 0 & 0 & 0 & 0 \\ 0 & -7.51 & 0.05 & 8.74 & -111.86 & -179.66 & -78.85 & 0 & 0 & 0 \\ 0 & 0.25 & 0.06 & -0.81 & -0.88 & 0 & 0 & 0 & 0 & -0.31 \\ 0 & 0.06 & 0.17 & 0.40 & -3.68 & 0 & 0 & 0 & 0 & 0.36 \\ 0 & 0 & -0.04 & -1.00 & 0 & 0 & 0 & 0.50 & 0 & 0 \\ 0 & 0 & -0.004 & 0 & -1.00 & 0 & 0 & 0 & 0.50 & 0 \\ 0 & 0 & 0 & 0 & 0 & 0 & 0 & 0 & 0 & 0 \\ 0 & 0 & 0 & 0 & 0 & 0 & 0 & 0 & 0 & 0 \\ 0 & 0 & 0 & 0 & 0 & 0 & 0 & 0 & 0 & 0 \end{bmatrix} \quad 3-33$$

$$B_u = \begin{bmatrix} 0 & 0 & 0 \\ 0 & 0 & 0 \\ -0.40 & -0.04 & 0 \\ -0.08 & 0 & 0 \\ 0 & -0.04 & 0 \\ 0 & 0 & 0 \\ 0 & 0 & 0 \\ 1.00 & 0 & 0 \\ 0 & 1.00 & 0 \\ 0 & 0 & 1.00 \end{bmatrix}$$

3.4 Controller design

This section presents the design of the controller. The proposed controller quasi SMC is explained in Section 3.4.1. The performance of the proposed controller was compared with LQR that is developed in Section 0. Both controllers were developed using the model developed in Section 3.3

3.4.1 Quasi Sliding Mode Control (QSMC)

The quasi SMC is also called the boundary layer technique used to reduce the chattering by approximate the signum function by introducing a boundary layer the movement on the sliding surface is relaxed and try to reach the sliding mode. The boundary layer was proposed by Slotine and Sastry in (Slotine & Sastry, 1983). The overall quasi design approach is summarised in Figure 3-3.

Consider the control law, and the sliding manifold for quasi SMC written in Equation 3-34 and 3-35 respectively

$$u = u_{eq} + u_{dis} \quad 3-34$$

$$\sigma = S\delta x(t) \quad 3-35$$

where $S \in R^{m \times n}$. Since the input matrix B is full rank, therefore sliding matrix S can be chosen such that SB is non-singular where $\det(SB) \neq 0$.

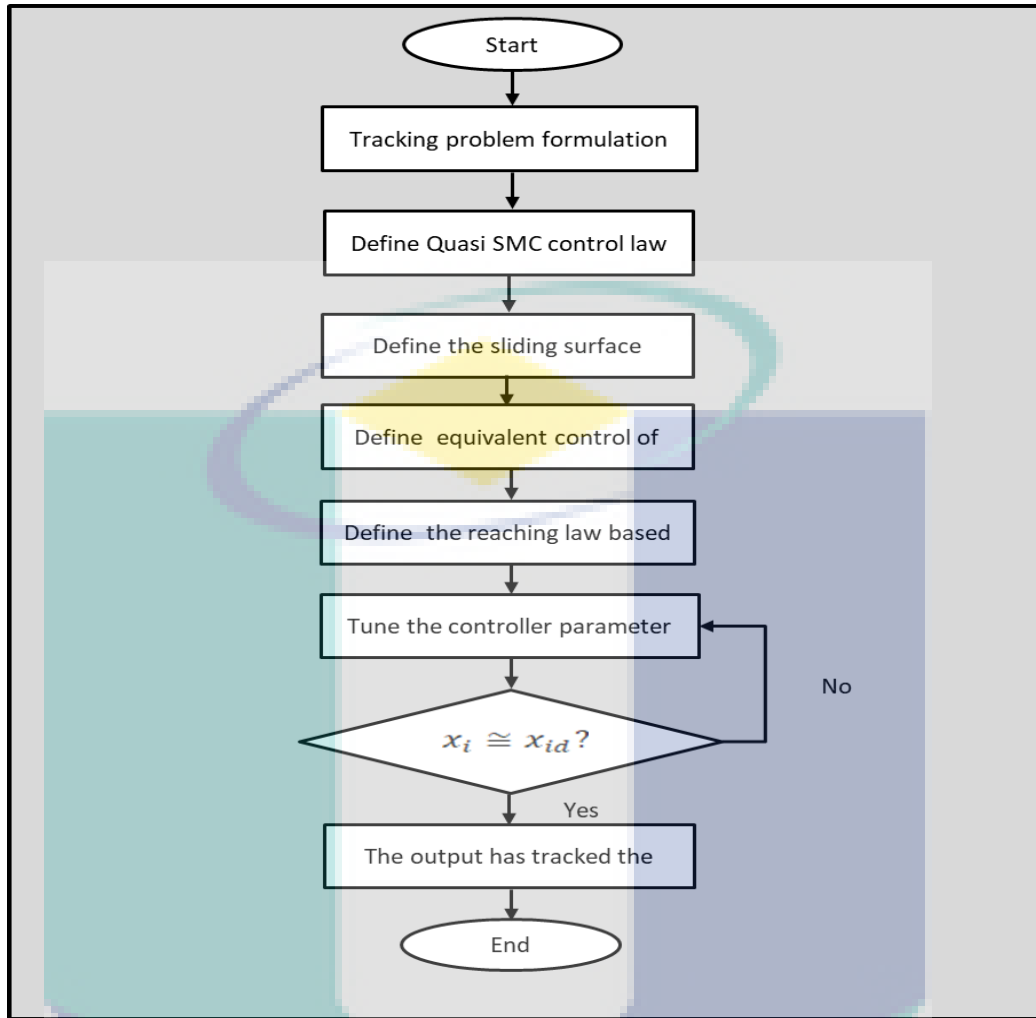


Figure 3-3 The flow of Quasi SMC design

The time derivative of sliding manifold is written as in Equation 4.102.

$$\dot{\sigma} = S\delta\dot{x}(t) \tag{3-36}$$

During the sliding $\sigma(t) = \dot{\sigma}(t) = 0$, and the equivalent control can be determined by substituting the Equation 3-30 into Equation 3-36). Therefore, the Equation **Error! Reference source not found.** becomes

$$\dot{\sigma} = S\delta\dot{x}(t) = S(A\delta x(t) + Bu(t) + Bh(x, t)) = 0 \tag{3-37}$$

and

$$u_{eq} = -(SB)^{-1}(SA\delta(x) + SBh(x, t)) \tag{3-38}$$

The reachability condition is chosen as boundary layer as written in Equation **Error! Reference source not found.**

$$u_{dis} = -M \frac{\sigma}{|\sigma| + \varepsilon} \quad 3-39$$

where M is a design parameter with positive value, and $\varepsilon > 0$ is the thickness of the boundary layer. Finally, the control law, u is written as

$$u = -(SB)^{-1}\{SA\delta(x) + SBh(x, t)\} - M \frac{\sigma}{|\sigma| + \varepsilon} \quad 3-40$$

Theorem 3.1: Consider the linear system in Equation 3-30 subjected to bounded uncertainty in Equation 3-31 with assumptions, the rank of B is full (i.e. rank(B)=m), the pair matrix A, and B is controllable, and the perturbation is matched to the input matrix B. If the sliding manifold, σ as written in Equation 3-35, and the control (u) as written in equation 3-40, then the convergence conditions are satisfied

Proof: Consider the lyapunov function Equation 3-41

$$V(\sigma) = \frac{1}{2} \sigma^2 \quad 3-41$$

The lyapunov time derivative along with Equation 3-37, yields

$$\dot{V}(\sigma) = \sigma \dot{\sigma} = \sigma \{S(A\delta x(t) + Bu + Bh(x, t))\} \quad 3-42$$

Substitute the Equation 3-40 into equation 3-42

$$\dot{V}(\sigma) = \sigma \left\{ M \frac{\sigma}{|\sigma| + \varepsilon} \right\} \quad 3-43$$

3.4.2 Linear Quadratic Regulator (LQR)

LQR is a method in modern control theory that uses state-space approach to analyse such a system. This the standard optimal control design which produces a stabilising control law that minimizes a cost function, J that is weighted of sum of squares of the states and input variables. Suppose we want to design state feedback control $u = Kx$ to stabilise the system. By determines the feedback gain matrix that minimises J, we can establish the trade-off between the use of control effort, the magnitude, and the speed of response that will guarantee a stable system. Assume that

all the states are available for feedback. The cost function to be minimised is defined as:

$$J = \int_0^{\infty} x(t)^T Q x(t) + u(t)^T R u(t) \delta t \quad 3-44$$

where Q is an $n \times n$ symmetric positive semi-definite matrix and R is an $m \times m$ symmetric positive definite matrix, (A, B) is stabilisable. Choosing Q relatively large than those of R , then deviations of x from zero will be penalised heavily relative to deviations of u from zero. On the other hand, if R is relatively large than those of Q , then control effort will be more costly and the state will not converge to zero as quickly as we wish.

3.5 Prototype development and system integration

This section presents in detail the prototype development and system integration of the AUG. The development of the glider prototype covers mechanical design and fabrication. In contrast, the system integration addresses the electronic components and embedded system development, which integrates the hardware and software to function together.

3.5.1 Mechanical design and fabrication

The body of the glider and the internal frame were fabricated by using aluminium alloy. On the other hand, the wings, tail wings and rudder were fabricated by using high density polyethylene (HDPE) polymer. Figure 3-4 shows the final prototype of the hybrid-driven AUG.

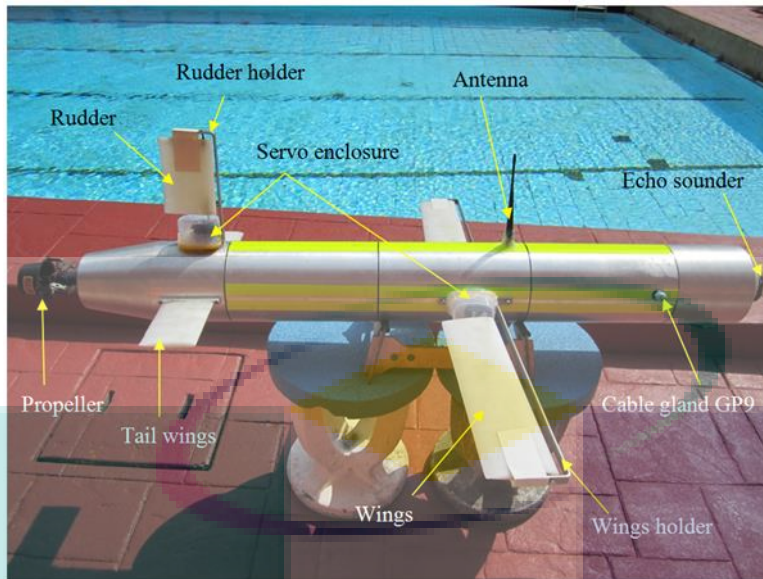


Figure 3-4 Final prototype of the autonomous underwater glider

The communication antenna for transmitting the GPS data to the surface workstation was added. The final prototype has two different servo motor enclosures.

3.5.2 Internal Frame

The internal frame contains all of the internal payloads such as the ballast pump, linear actuator for sliding mass, the sensor module, microcontroller module, the communication module, power module, data logger module and additional mass. The internal frame was divided into two levels: lower level and upper level. In order to make the CG of the glider as low as possible, all the heavy components such as the ballast pump, sliding mass and battery packs of the power module were placed at the lower level. On the other hand, the lighter parts such as a microcontroller, sensor, communication and data logger module were placed at the upper level of the frame. Placing the payloads by using this approach would make the glider stable and would prevent it from turning upside down easily. Figure 3-5 shows the internal frame of the glider.

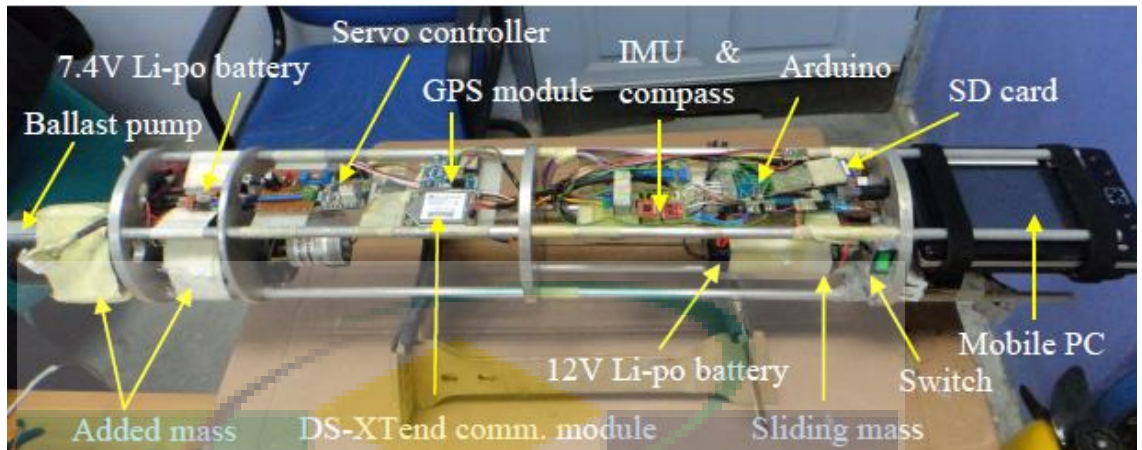


Figure 3-5 Internal frame of the AUG

3.5.3 Ballast tank

Piston tank TA825 was used as the ballast pump of the glider. The ballast pump was located at the far front of the internal frame by inserting half of the pump inside the pocket of the first and second discs of the internal frame. In order to make the ballast pump able to suck in water from the outside of the glider's body, a water-tube was connected from the tube socket on the pump to the cable gland GP9. The piston tank TA825 was chosen to control the depth of the glider because it was easy to install and use. However, the installation of this tank requires sufficient space for the tank and also the spindle, which is driven outwards and inwards during operation. This tank has a DC motor and three limit switches, and requires 12V of power to operate. The first limit switch will turn OFF if the tank is empty, whereas the second and third limit switches will turn ON if the tank is full and 85% full, respectively. Thus, a control circuit is required to control the DC motor according to the output from the limit switches. Figure 3-6 shows the ballast pump installation and configuration.



Figure 3-6 Ballast tank installation and configuration

3.5.4 Internal movable sliding mass

The internal sliding mass has been designed by using the digital linear actuator 26DBM10D2U-L. The linear actuator was attached to a square aluminium plate, which has 10 cm of length, 10 cm of width, and 1 cm of height. This linear actuator moves along a threaded rod, which was installed between the third and fourth discs of the internal frame. In order to ensure that the sliding mass aluminium plate was stable, two aluminium rods were used to support the plate. Three 12V Li-Po batteries were placed on top of the aluminium plate as the sliding mass. The overall length of the linear actuator of the sliding mass is 494.55 mm, where the distance or travel length for the mass is 300 mm. Figure 3-7 presents the sliding mass installation, and Figure 3-8 shows the bottom view of the internal movable sliding mass.

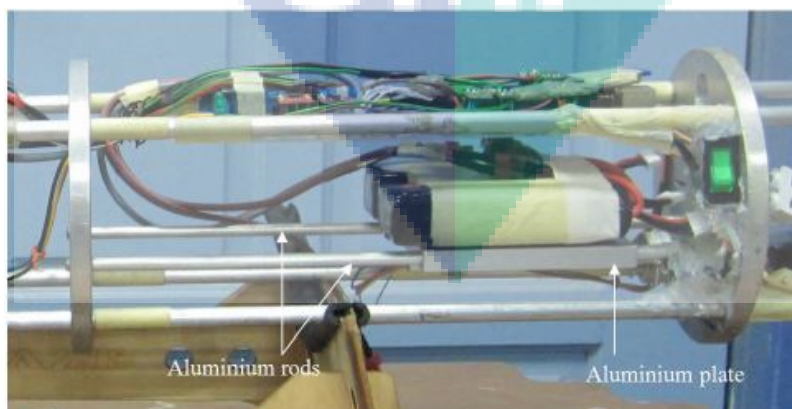


Figure 3-7 Internal movable mass installation

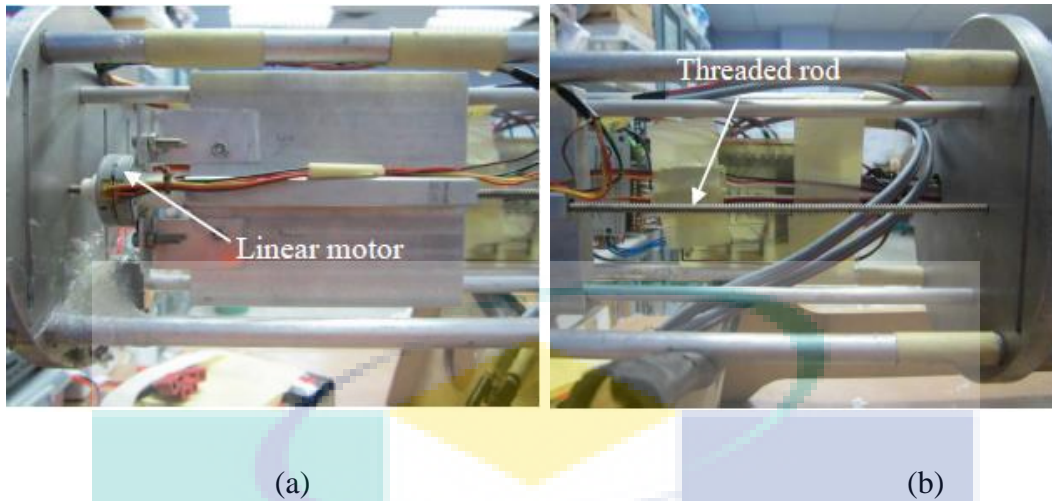


Figure 3-8 Bottom view of the internal sliding mass (a) Linear motor and (b) Threaded rod

3.6 Electronic components and system integration

This section presents the electronic system of the glider as well as the hardware-software integration. In order to make all of the electronic and mechanical components fully functional, the programming code for the components was designed. The discussion of the system integration covers a controller module, a sensor module, an internal actuator module, an external actuator module, a communication module, and a data logger module.

3.6.1 Controller module

The controller module was divided into two parts: the main controller and the peripheral controller. The Arduino Mega 2560 was selected as the main microcontroller for the glider. It was chosen because it is an open-source platform, which is easy to use for hardware-software integration. Furthermore, it has all of the required pins or ports such as digital and analogue input/output pins and UART (serial) ports, to support the operation of the glider. The Arduino Integrated Development Environment (IDE) is used to program the microcontroller based on the Arduino programming language. Figure 3-9 shows the controller module of the glider.

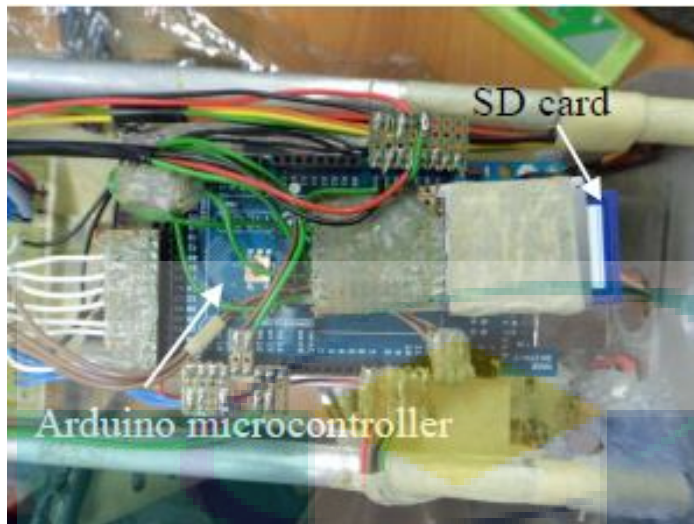


Figure 3-9 Controller module

The program of the controller algorithm was designed using MATLABTM; due to this, the program cannot be uploaded into the Arduino microcontroller. However, the Arduino is able to communicate with MATLABTM through serial communication. In order to make MATLABTM able to communicate with the Arduino, the Arduino program first had to be uploaded into the Arduino and then executed the MATLABTM program. Figure 6.13 shows the MATLABTM code to communicate with the Arduino, read the sensor data, and send the control input to the Arduino. On the other hand, Figure 3-10 shows the Arduino code to read data from MATLABTM.

UMP

```

243 %% Arduino to Matlab
244 numSec=100; t=[]; data=[];
245
246 s1 = serial('COM12'); %define serial port
247 s1.BaudRate=9600; %define baud rate
248
249 fopen(s1);
250 fileID = fopen('HybridRolling.txt','a+');
251
252 clear data; i=0; t0=tic;
253 while (toc(t0)<=numSec)
254
255     i=i+1; t(i)=toc(t0); t(i)=t(i)-t(1);
256
257     time(i,:)=fscanf(s1,'%f'); heading(i,:)=fscanf(s1,'%f');
258     pitch(i,:)=fscanf(s1,'%f'); roll(i,:)=fscanf(s1,'%f');
259     pitch_rate(i,:)=fscanf(s1,'%f'); roll_rate(i,:)=fscanf(s1,'%f');
260     yaw_rate(i,:)=fscanf(s1,'%f'); temperature(i,:)=fscanf(s1,'%f');
261     depth_sensor(i,:)=fscanf(s1,'%f'); front_sensor(i,:)=fscanf(s1,'%f');
262     latitude(i,:)=fscanf(s1,'%f'); longitude(i,:)=fscanf(s1,'%f');
263
264     T = i;
265     [y3, t3, u3] = sim(Homeobj, T, r, v, simopt); %homeostatic
266
267     fprintf(s1,'%f',abs(u3(i,4)));
268     fprintf(s1,'%c',' ');
269     fprintf(s1,'%f',abs(u3(i,1)));
270
271 end
272 fclose(s1);

```

Figure 3-10 MATLAB™ to communicate with the Arduino through serial Communication

```

while( Serial.available() > 0){
    char c=Serial.read();

    if ((c!=' ') && (readString.length()<11))
        readString.concat(c);
    if ((readString.length()>10) && (readString1.length()<10))
        readString1.concat(c);

    netforce_ux = readString.toFloat();
    wing_angle = readString1.toFloat();

    readString=""; //empty for next input
    readString1="";
}

```

Figure 3-11 Arduino code to read from MATLAB™.

3.6.2 Sensor module

The sensor module for the glider system consists of an IMU sensor, compass, echo sounder and GPS. The IMU SEN10121 was used to measure the glider's pitch angle, roll angle, and acceleration or angular velocity. The SEN10121 is a simple 6-DOF sensor that has an ADXL345 accelerometer and an ITG-3200 gyro. This sensor communicates with the Arduino microcontroller through the I2C output pin. I2C is a two-wire interface consisting of serial data signal (SDA) and serial clock (SCL). Figure 3-12 shows the IMU and compass sensor of the glider system.



Figure 3-12 IMU and compass

On the other hand, the digital compass HMC6352 was used to measure the heading, or yaw angle, of the glider. This fully integrated compass combines 2-axis magneto-resistive sensors with the analogue and digital support circuits, and algorithms for heading computation. The compass also communicates via a two-wire I2C serial interface. These sensors are small, with low-power voltage, where the voltage can be supplied directly by the Arduino Mega board. The supply voltage for the IMU is 2.0 Vdc to 3.6 Vdc, whereas the supply voltage for the compass is 3.3 Vdc.

Two echo sounders have been installed on the glider's nose vertically and horizontally. Each echo sounder has an ATU120BT active transducer. The vertical echo sounder measures the depth between the glider and seabed, and the horizontal echo sounder measures the distance between the glider and obstacle. These active transducers produced NMEA 0183 serial data of depth and water temperature, and operate at 120 kHz with power voltage of 12 V. In order to read and log the depth and temperature, the Arduino program for reading the NMEA data from the echo sounders had to be uploaded into the Arduino Mega board. The Arduino will continuously received the

data and compared with the specific NMEA ASCII characters. If the data was matched with the ASCII characters, then Arduino read the next data.

The GPS was used to measure the location of the glider in terms of latitude and longitude. SKGPS-53 was chosen as the GPS module because of its ultra-high sensitivity and high-performance navigation. The SKGPS-53 sent the glider's location continuously to the surface workstation through the DS-XTend antenna. Thus, the surface workstation received the data when the glider rose to surface. In order to program the GPS module with the Arduino via serial communication, the TinyGPS and SoftwareSerial library was downloaded into the Arduino/Libraries folder. Figure 6.16 shows the SKGPS-53 module.

3.6.3 Internal Actuator module

The internal actuator module consists of the ballast pump and sliding mass. The piston tank TA825 was used as a ballast pump for the glider, which required 12V of power. Thus, a 12V Li-po battery was used as a power source for the pump. A control circuit was designed to control the direction of the ballast spindle through the provided DC motor. The DC motor will automatically stop when the tank is either empty or full. The Arduino program code for the ballast pump is straightforward, meaning that the Arduino just assigns high or low output signal to the control circuit. Figure 3-13 shows the ballast pump control circuit.

In order to make the sliding mass able to move forward and backward, the digital linear actuator 26DBM10D2U-L was used. A 12 V Li-po battery was used as the power source, and four transistors were used for amplifying the signal from Arduino, because this output signal was only 5 V. An Arduino Stepper library was used to program the linear actuator so that the actuator was able to slide back and forth through the threaded rod. Figure 3-14 shows the control circuit for the linear actuator of the sliding mass.

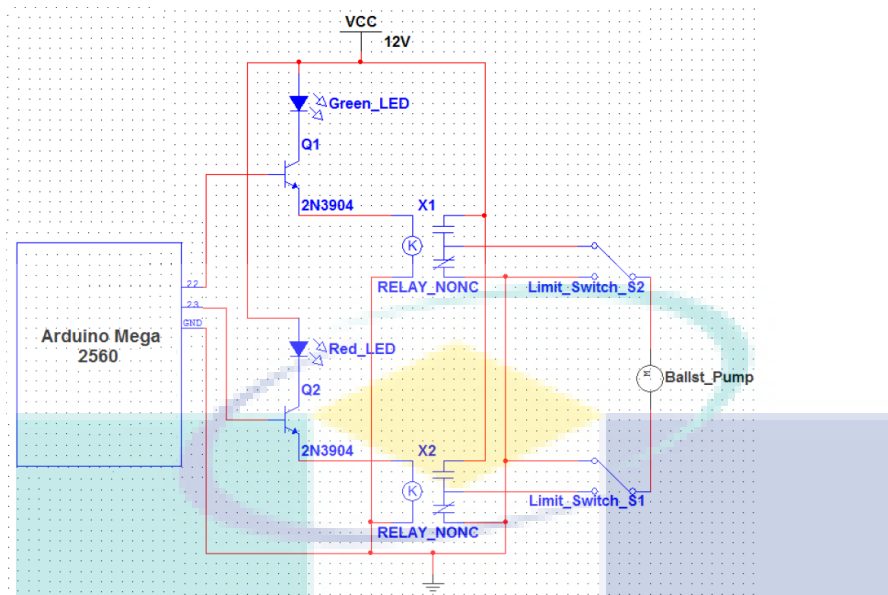


Figure 3-13 Ballast pump control circuit

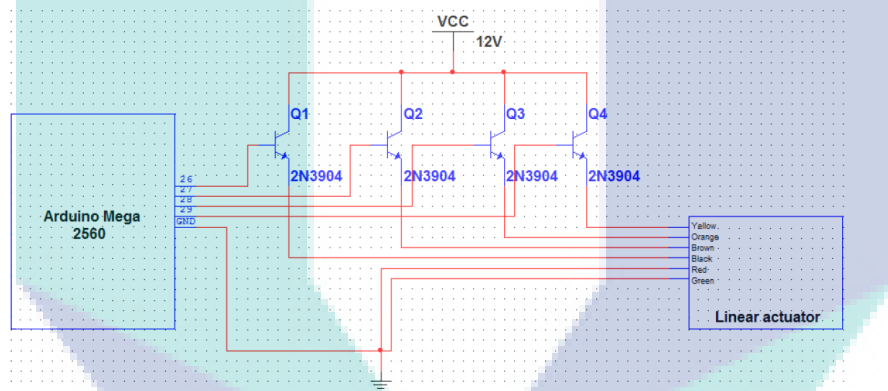


Figure 3-14 Linear actuator control circuit

3.6.4 Communication module

A DS-XTend RF module was used as a communication module for transmitting the glider location to the surface workstation. This RF module is an easy-to-use module that provides reliable delivery of critical data between remote devices. It transfers a standard asynchronous serial data stream, which operates within the ISM 900 MHz frequency band and is able to send 115.2 Kbps data. The module required 2.8V to 5V supply voltage. Thus, the power supply for the XTend is provided by the Arduino board. In order to send the GPS data, the XTend communication pins must be connected to the Arduino's serial communication pin. Figure 3-15 shows the XTend RF module.



Figure 3-15 The DS-XTend RF module

3.6.5 Data logger module

The glider system has two types of data loggers. The primary data logger is the SD card, and the secondary data logger is the mobile PC. The SD card was connected to the Arduino digital pins and communicated with the Arduino through the Serial Peripheral Interface (SPI). In addition, the hardware SS pin had to be used to select the SD card. The program code of the SD card required the Arduino SD library. This library allows reading and writing data to the SD card. On the other hand, the program for the secondary data logger was designed inside the complete MATLAB™ program of the homeostatic controller algorithm. The program saves the data inside the hard disk of the mobile PC. Each sensor data parameter (such as pitch angle, roll angle and heading angle) was saved in its own text file inside the SD card. In addition, the overall sensor data was also saved in the SD card and the mobile PC. Figure 3-16 shows the SD card data logger.

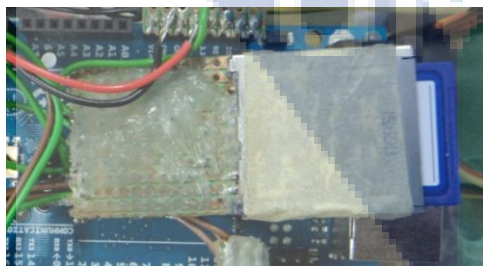


Figure 3-16 SD card data logger

CHAPTER 4

RESULTS AND DISCUSSION

4.1 Introduction

In this chapter, the results and discussions of the research works are discussed and presented. The results will be discussed the tracking performance of the proposed controller. The tracking performance will be evaluated in terms of settling and experimental result of the developed AUG.

4.2 Performance of sliding mode control

The Quasi SMC was designed for the nonlinear equations of an AUG longitudinal plane that has been presented in Chapter 3. The control system consists of three inputs and ten outputs. However in this study, there were only two outputs considered which are pitching angle (θ), gliding angle (ξ), horizontal (v_1) and vertical velocities (v_3) are observed. The simulations were done using the parameters adopted from Graver, (2005) as depicted in Table 4-1

Table 4-1 Parameter values of the AUG

Parameter	Value	Unit
Hull mass, m_h	40	kg
Internal sliding mass, m_p	9	kg
Displaced fluid mass, m_{df}	50	kg
Added mass, m_{f1}, m_{f2}, m_{f3}	5, 60, 70	kg
Inertia, J_1, J_2, J_3	4, 12, 11	kgm ²
Lift coefficient, K_{L0}, K_L	0, 132.5	-
Drag coefficient, K_{D0}, K_D	2.15, 25	-
Moment coefficient, K_{M0}, K_M	0, -100	-
Constant coefficient, $K_{\omega_1^2}, K_{\omega_2^2}$	50, 50	-

The proposed controller was developed and simulated using MATLABTM. The block diagram of a quasi SMC algorithm is shown in Figure 4-1. The simulations have been carried out for the glider to glide from -25° to 25° . The initial values of the states and desired observed outputs are depicted in Table 4-2. All the controller gains are heuristically tuned. The parameter p in continuous part of super twisting sliding mode in Equation (4.75) is chosen as 0.5 to ensure maximum real sliding order of super twisting realisation is achieved as suggested by various previous works (Bartolini et al., 1999; Arie Levant & Fridman, 2002; Arie Levant, 2007; Salgado-Jimenez & Jouvencel, 2003). The proposed controller parameter values are depicted in **Error! Reference source not found.**

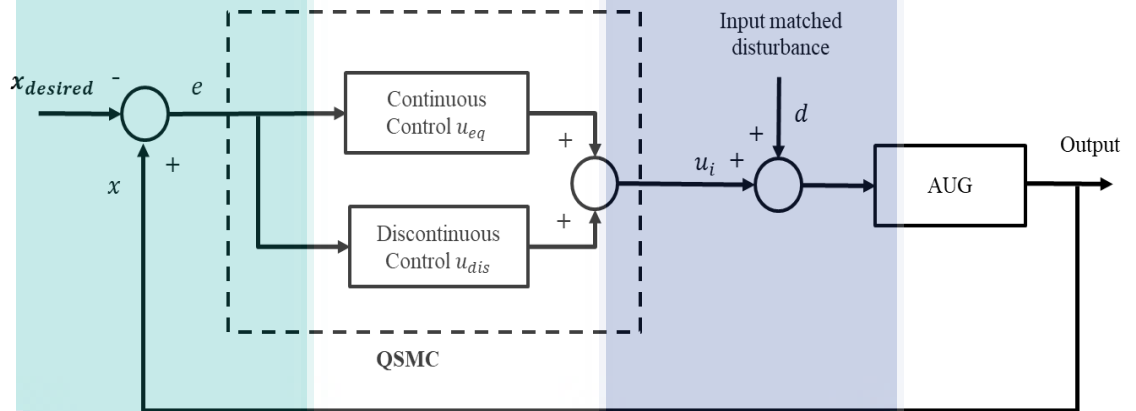


Figure 4-1 The block diagram of a QSMC

Table 4-2 The initial and desired values of the states

Parameter	Initial	Desired
Gliding angle, θ	-45°	45°
Surge velocity, v_1	0.3 ms^{-1}	-
Heave velocity, v_3	0.02 ms^{-1}	-
x- position of internal mass, r_{p1}	1.98 cm	-
Ballast mass, m_b	1.05 kg	0.95 kg
Excess mass, m_{em}	0.05 kg	-0.05 kg

The QSMC controller parameters and sliding manifolds for gliding down and gliding up are written in Equation 4-1 and 4-2 respectively.

$$S_d = \begin{bmatrix} 20 & -17 & -19 & -20 & 75 & 440 & 15 & -199 & 10 & 1 \\ -17 & 7 & 10 & 5 & -50 & -2300 & 110 & -5 & 7 & -1 \\ -2 & -1 & -2 & 15 & 10 & 55 & -24 & 2 & -0.3 & 10 \end{bmatrix} \quad 4-1$$

$$M_d = 100, \varepsilon_d = 0.1$$

$$S_d = \begin{bmatrix} 0.2 & 2 & -2.5 & -28.4 & -36 & 440 & 15 & -199 & 10 & 1 \\ -17 & 7 & 10 & 5 & -50 & -230 & 110 & -5 & 7 & -1 \\ -2 & -1 & -2 & 15 & 10 & 55 & -24 & 2 & -0.3 & 10 \end{bmatrix} \quad 4-2$$

$$M_u = 100, \varepsilon_u = 0.01$$

The LQR controller parameters for gliding down and gliding up are written in Equation 4-3 and 4-4 respectively.

$$K_{dLQR} = \begin{bmatrix} 24.05 & -10.36 & -13.49 & -22.98 & 114.37 & 319.97 & -137.59 & 11.30 & -2.84 & 2.18 \\ -14.84 & 5.96 & 8.41 & 8.87 & -77.59 & -204.16 & 94.24 & -3.85 & 5.29 & -0.52 \\ -1.13 & -0.28 & -0.14 & 7.86 & 23.77 & 64.36 & -28.47 & 1.91 & -0.50 & 8.00 \end{bmatrix} \quad 4-3$$

$$Q_d = \text{diag}(800,500,200,200,50,50,20,10,10,50)$$

$$R_d = \text{diag}(1,1,1)$$

$$K_{uLQR} = \begin{bmatrix} 0.69 & 1.09 & -0.64 & -11.56 & 13.87 & 53.72 & 23.55 & 6.16 & 2.49 & 2.03 \\ 0.10 & 0.33 & -0.08 & -3.59 & 2.40 & 13.55 & 6.28 & 1.65 & 1.94 & 0.57 \\ 0.10 & 0.28 & -0.22 & -4.03 & 5.05 & 17.96 & 7.78 & 1.63 & 0.76 & 1.31 \end{bmatrix} \quad 4-4$$

$$Q_u = \text{diag}(0.5,0.5,1,2,2,0.1,0.1,1,1,0.05)$$

$$R_u = \text{diag}(1,1,1)$$

The performance of proposed controller for the gliding down is shown in Figure 4-2 to Figure 4-5 and Figure 4-6 to Figure 4-9 for upward glide. The QSMC able to stabilise at desired value within 7 seconds for gliding angle, 9 seconds for pitching angle, 5.2 seconds for horizontal velocity and 13 seconds for vertical velocity during

the downward glide. However, the LQR took longer time about two times slower than QSMC. As for upward glides the QSMC able to stabilise at the desired value faster than LQR. The summarised of the performance is depicted in Table 4-3.

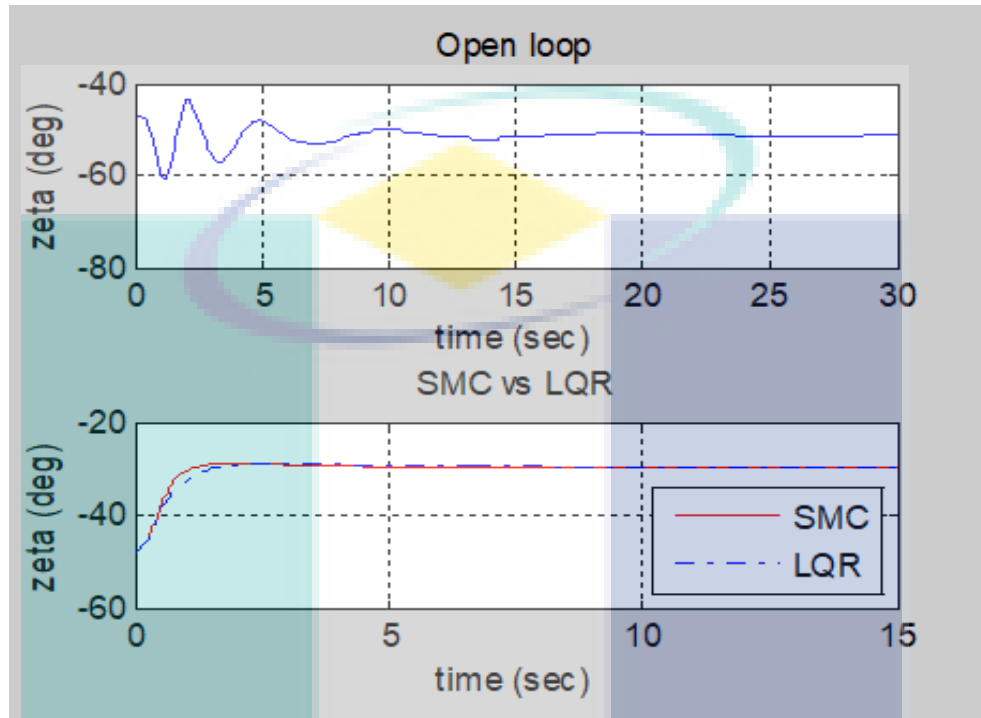


Figure 4-2 Gliding angle, ζ (downward glide)

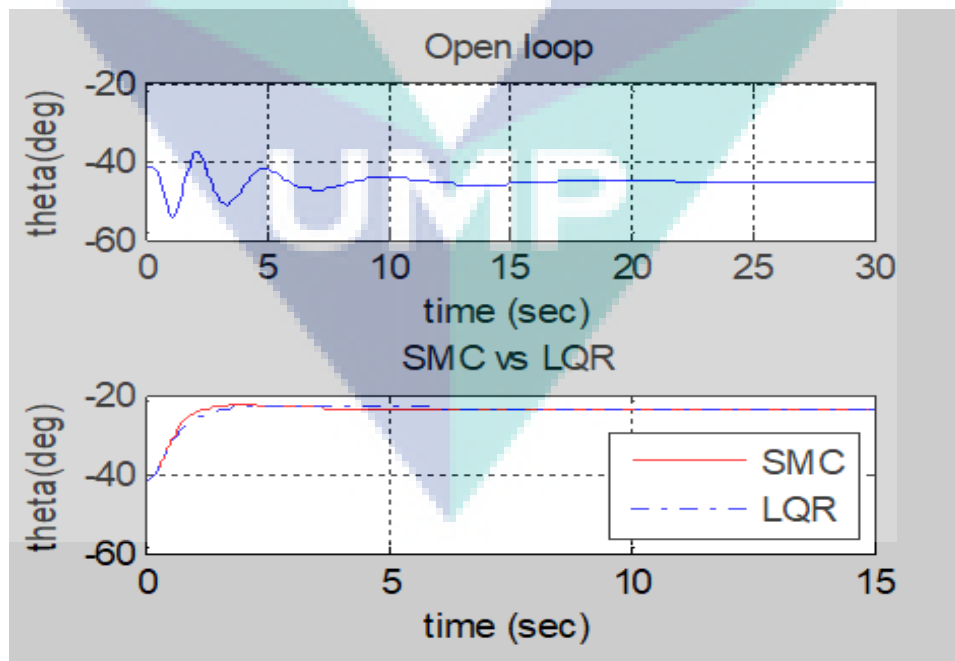


Figure 4-3 Pitching angle, θ (downward glide)

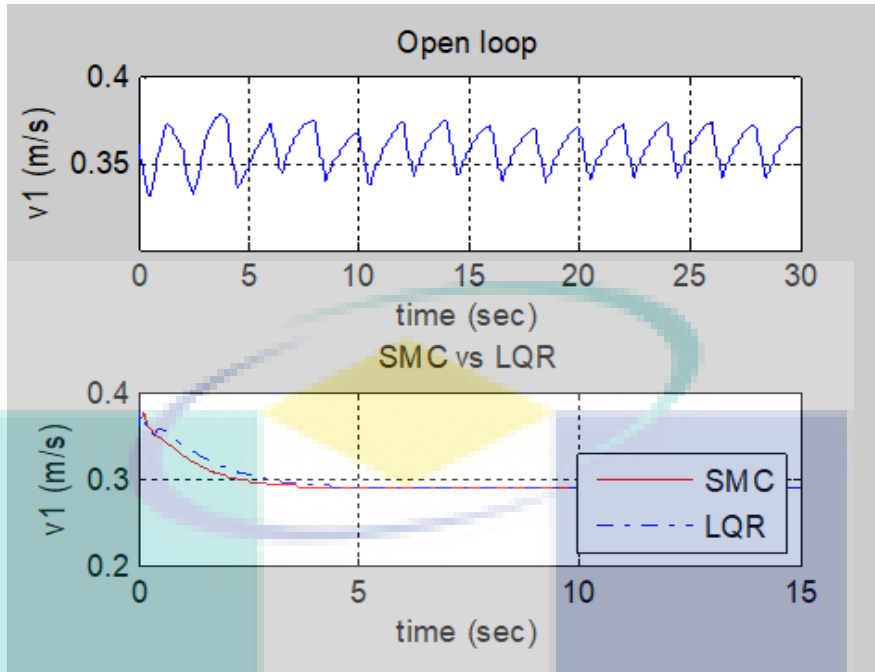


Figure 4-4 Horizontal velocity, v_1 (downward glide)

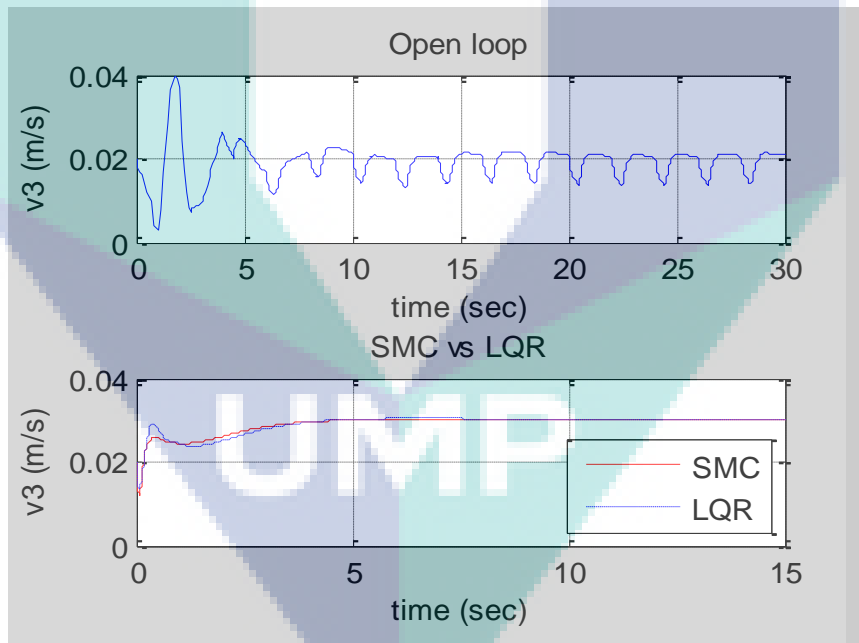


Figure 4-5 Vertical velocity, v_3 (downward glide)

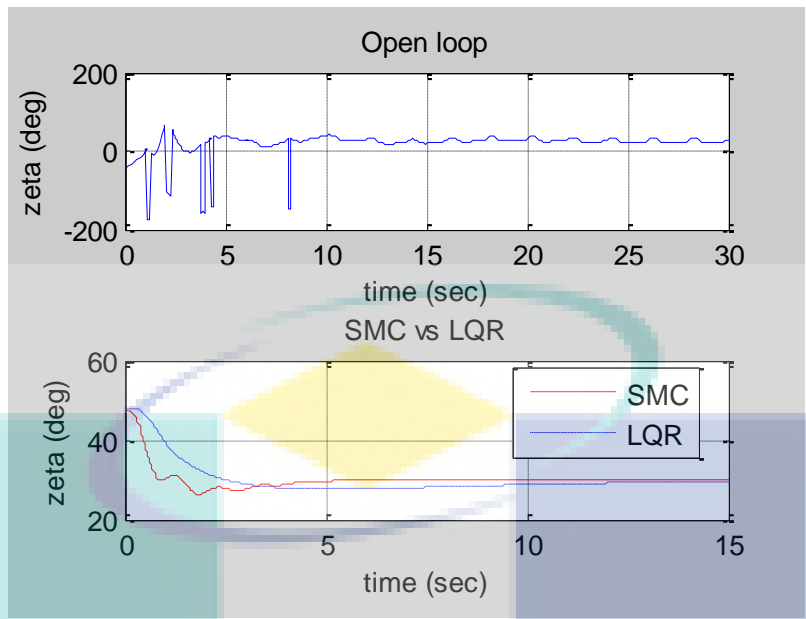


Figure 4-6 Gliding angle, ξ (upward glide)

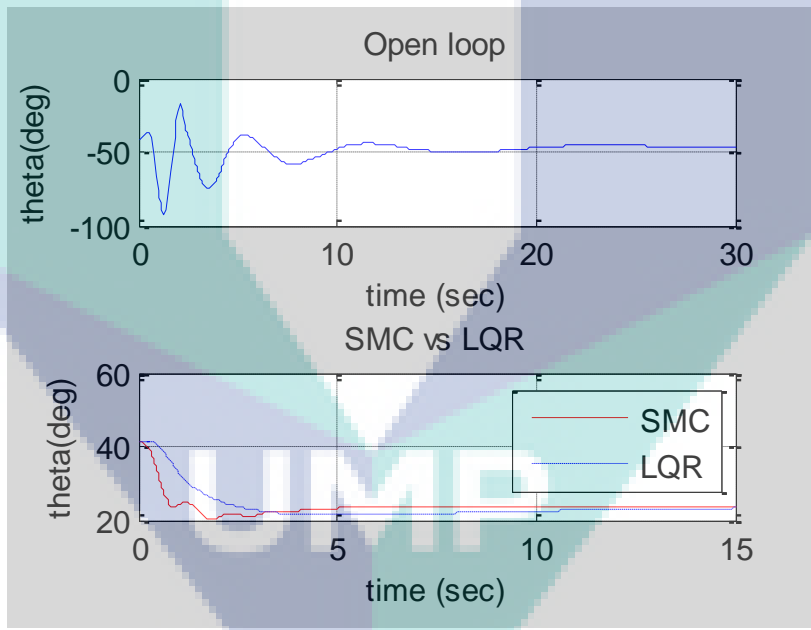


Figure 4-7 Pitching angle, θ (downward glide)

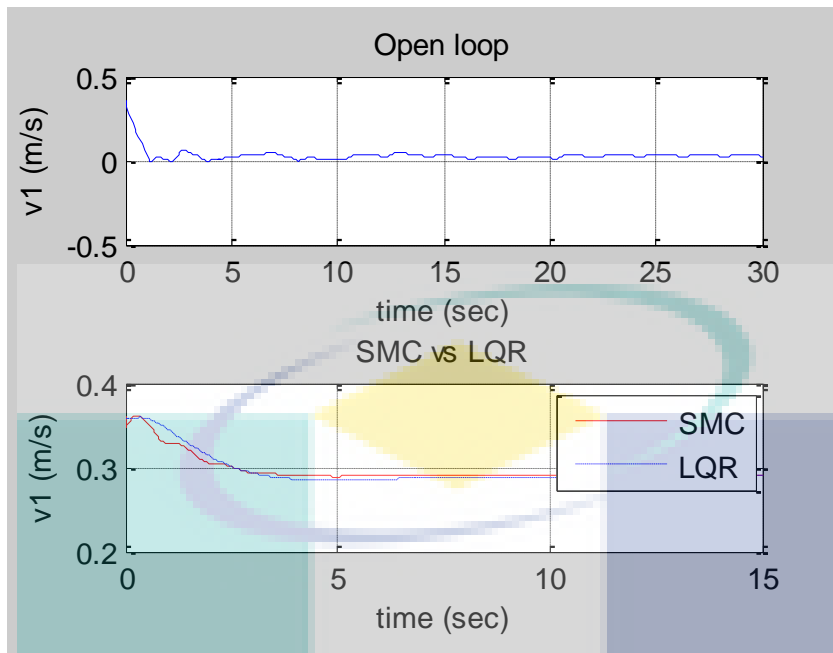


Figure 4-8 Horizontal velocity, v_1 (upward glide)

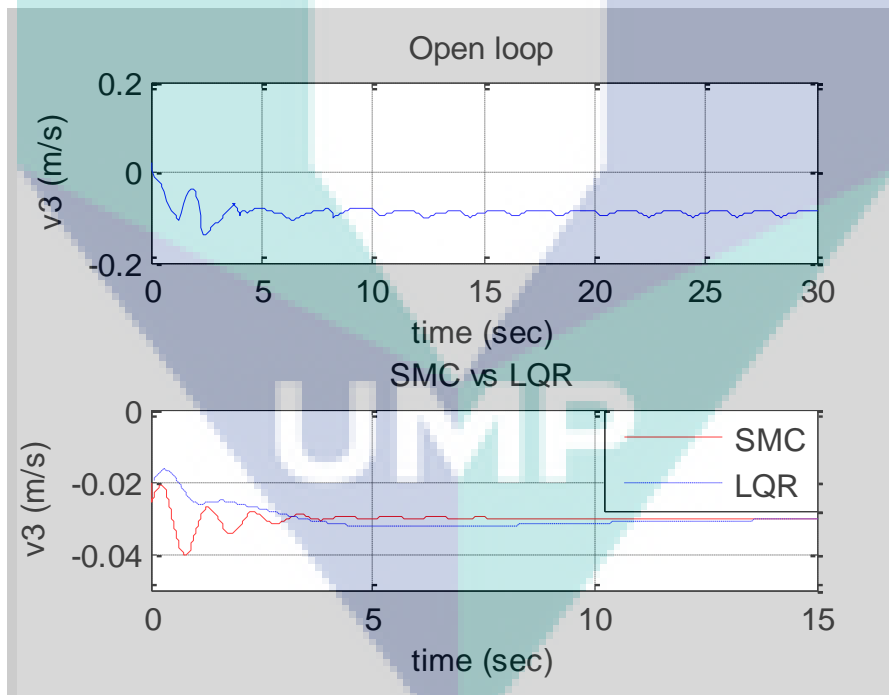


Figure 4-9 Vertical velocity, v_3 (upward glide)

Table 4-3 Summary of controllers' performances

Output tracking	QSMC (sec)		LQR (sec)	
	DOWN	UP	DOWN	UP
Gliding angle (deg), ξ	7	8	11.5	24
Pitching angle (deg), θ	9	10	12	25
Horizontal velocity (m/s), v_1	5.2	5	5	10
Vertical velocity (m/s), v_3	13	8	6	20

4.3 Prototype testing and experimental

The prototype testing was conducted after the system of the hybrid-driven AUG had been completely developed. However, several preliminary tests such as waterproof and buoyancy tests had to be performed before the real-time experimental tests. These two preliminary tests are very important, because without the proper initial buoyancy level and waterproof capability, the glider will fail to operate successfully.

4.3.1 Water proof and buoyancy test

The waterproof test was conducted out inside a water tank in order to protect the electronic components inside the glider from damage due to water leakage. The glider had been submerged into the water inside the water tank for several hours to check for the occurrence of water leakage. In addition, the buoyancy test inside the water tank was also performed. In order to prevent water leakage, rubber grease was applied at the screw thread of the hull, nose and rudder. the glider was tested in both a static condition and a mobile condition, in order to verify that the glider was completely free from water leakage. As a result, it was found that the glider was free from leakage, but the plastic enclosure for the servo motors always suffered from water leakage. Thus, the plastic enclosure of servo motors had to be refabricated and reinstalled each time before the test. Figure 4-10 shows the waterproof test as well as the buoyancy test inside the water tank.

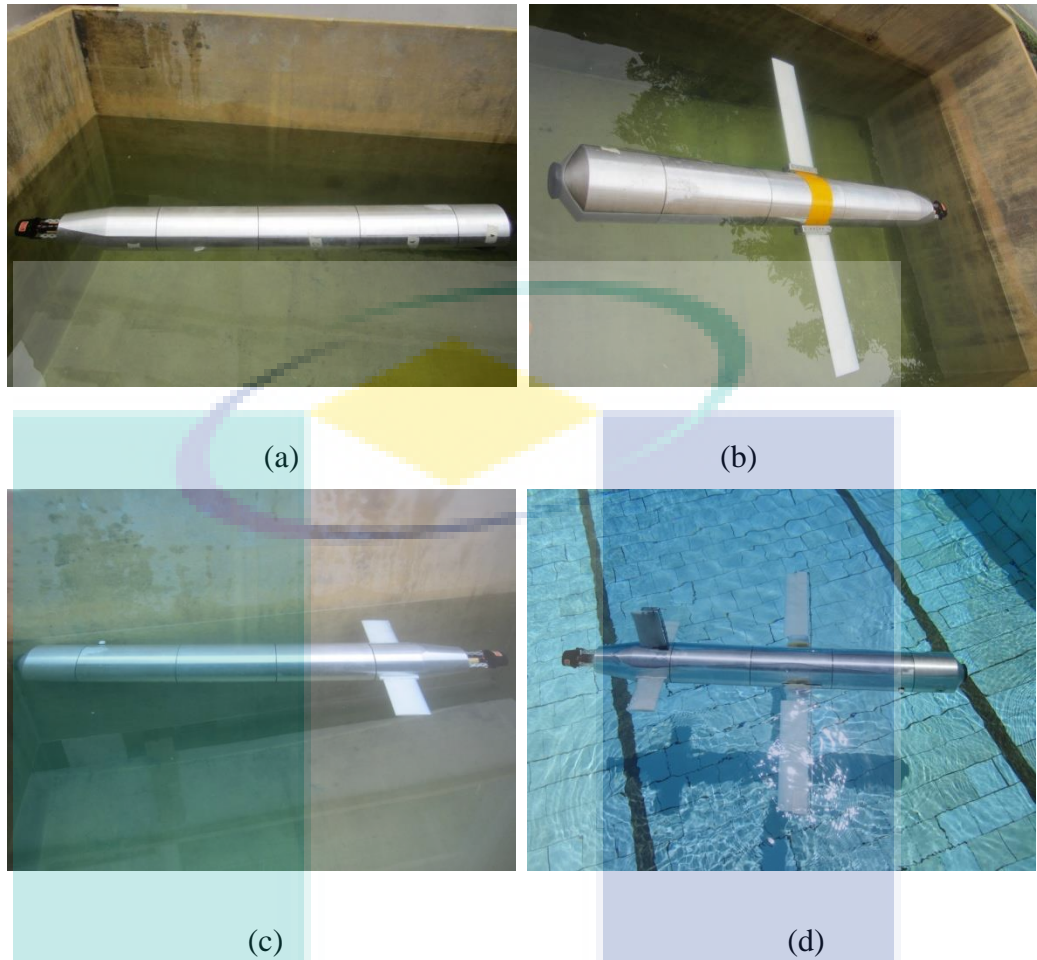


Figure 4-10 Waterproof and buoyancy test: (a) test without wings and tail wings inside water tank, (b) test with wings, (c) test with tail wings, (d) test with complete glider.

The buoyancy test was carried out in order to verify that the glider had nearly zero buoyancy force as its initial state. The buoyancy test was performed by throwing the glider into the water and observing whether the glider was sinking or floating. The buoyancy level of the glider was expected to be slightly below the water surface. However, without additional weights the whole body of the glider did not completely submerge. As a result, by adding the mass, the glider showed slightly positive buoyancy, was stable when floating, and the whole body was able to be submerged into the water without sinking to the bottom.

4.3.2 Functionality and reliability test

The functionality and reliability tests were performed for the compass module, IMU sensor, echo sounder, GPS module, DS-Xtend antenna, ballast pump, internal sliding mass, wings, rudder and propeller. These tests are important in order to allow the glider to operate successfully during the sea trial and real-time system test.

The yaw or heading angle is important in order to control the heading of the glider. Thus, the compass module was calibrated before testing its functionality and reliability. The purpose of this test was to check whether the compass sensor was able to gather reliable information about the yaw or heading angle. Figure 4-11 shows the result of the compass module reliability test. Basically, the initial value of North is $0^{\circ}/360^{\circ}$, and the value increased when the direction is turned counter-clockwise. The maximum heading value given by the compass was 359.9° . For consistency purpose, the compass reading was taken 20 times.

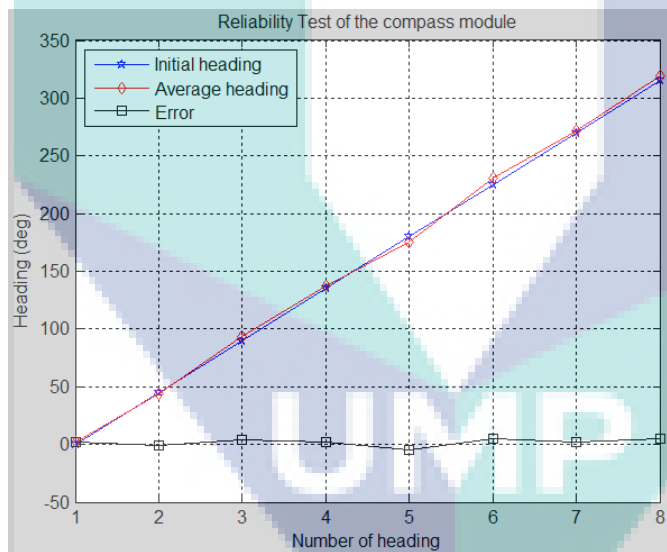


Figure 4-11 Compass module reliability test

The functionality and reliability of the IMU test are also important because the roll and pitch angles provided by the IMU were used to control the gliding and rolling motion of the glider. The purpose of this test on the IMU was to measure whether the IMU gives a correct measurement of these angles. Initial value for the roll and pitch angle of the glider was 0° when the glider was horizontally straight. The value of roll angle was positive when the glider was rolling to the right side, whereas the IMU

produced a negative value of the pitch angle when the glider was gliding downward, and vice-versa. Similar to the heading angle evaluation, the measurement of these angles was taken 20 times. Figure 4-12 and Figure 4-13 show the results of the IMU reliability test of the roll and pitch angles, respectively.

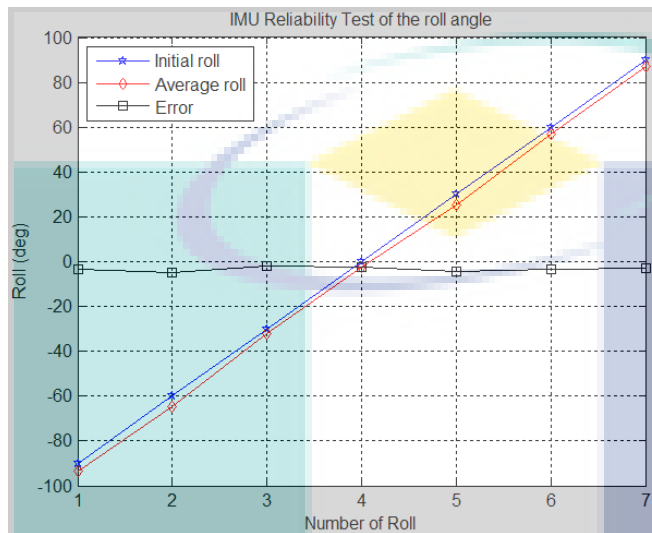


Figure 4-12 IMU reliability test of the roll angle

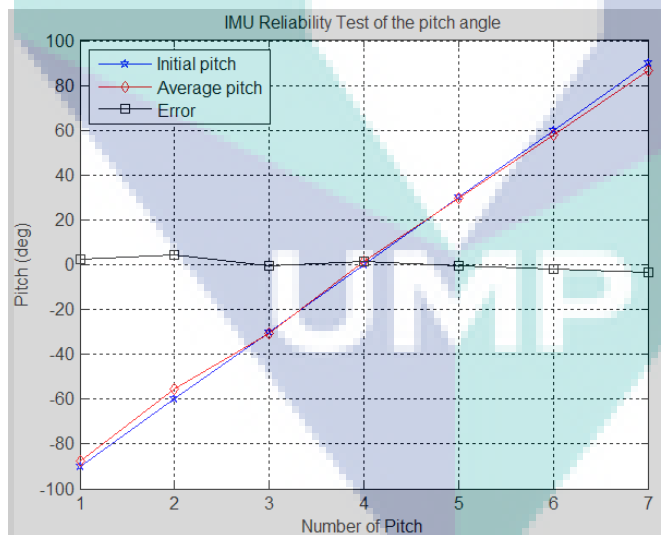


Figure 4-13 IMU reliability test of the pitch angle

The GPS module, DS-Xtend communication, and DS-Xtend antenna work together in order to send the GPS data to the surface workstation through the Arduino. The functionality test of these components is important, in order to ensure that the GPS module is able to gather the glider location and transmit it to the workstation. Beside

transmitting the GPS location to the surface workstation, the location data is also logged by the data logger as a record. Figure 4-14 shows the DS-Xtend module and transmitter antenna that is able to transmit the GPS data to the workstation and the receiver antenna able to receive the data. In this figure, the GPS location was zero because it was tested in the lab where the GPS module was not able to gather the data from the GPS satellite.

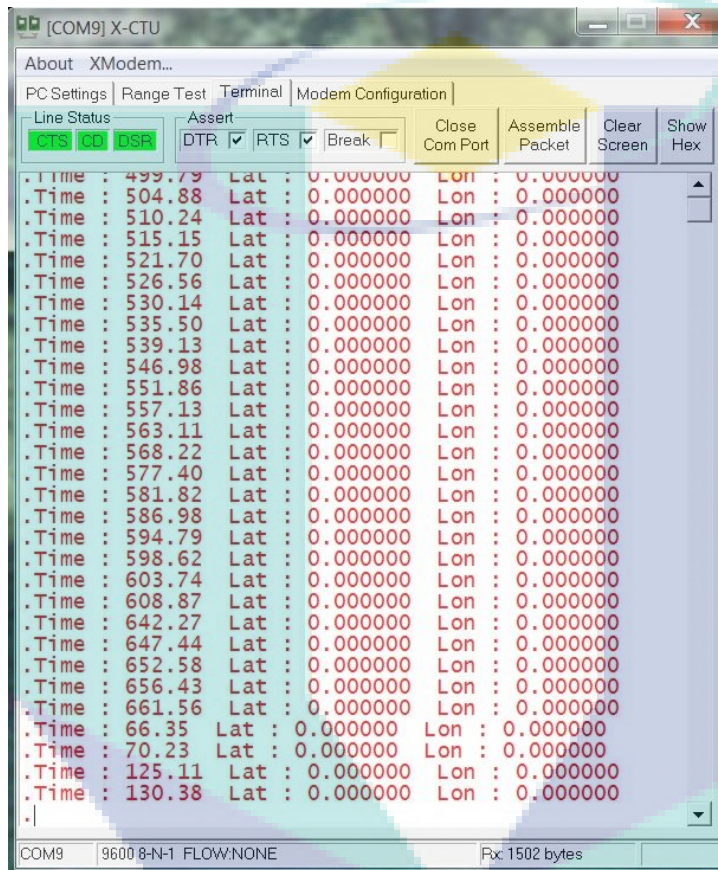


Figure 4-14 Transmitted GPS data

The functionality of ballast pump is important because it was used to control the buoyancy of the glider. However, since the ballast pump was located at the front of the glider, the variable mass of the ballast pump will also affect the pitch angle of the glider indirectly. The ballast pump has a piston that is attached to a threaded rod. In order to move the piston forward and backward for pumping the water in and out, the threaded rod was rotated by the DC motor. Figure 4-15 shows the threaded rod for pumping in the water.

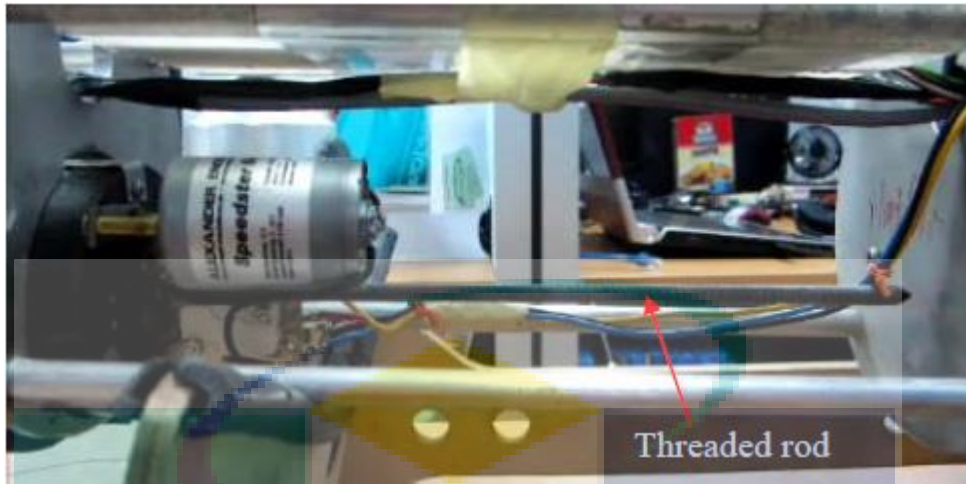


Figure 4-15 Threaded rod of the ballast pump

The functionality of the internal sliding mass is important in order to control the pitch angle of the glider. It has a fixed mass but a variable position. The fixed mass originates from the mass of three 12V Li-po batteries and also from the aluminium plate. Its power consumption is 3.4 W, and its speed is fixed. Figure 4-16 shows the initial position and the maximum position of the sliding mass.

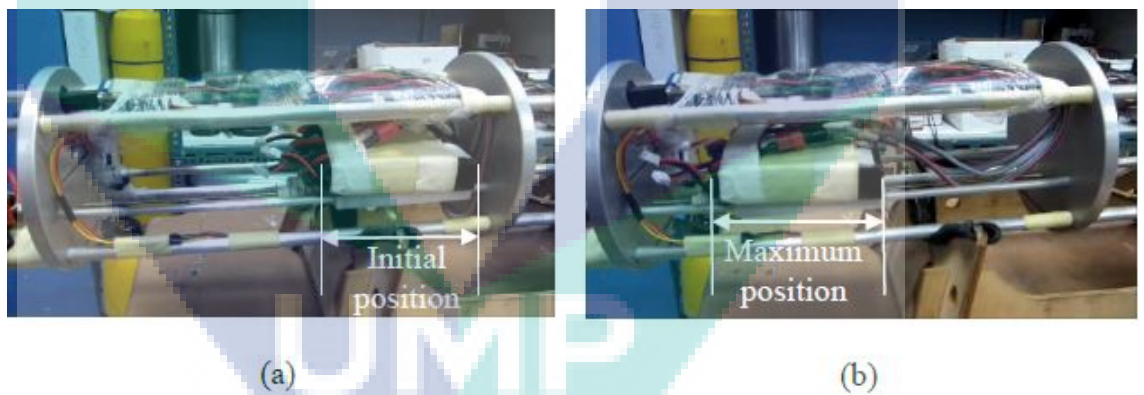


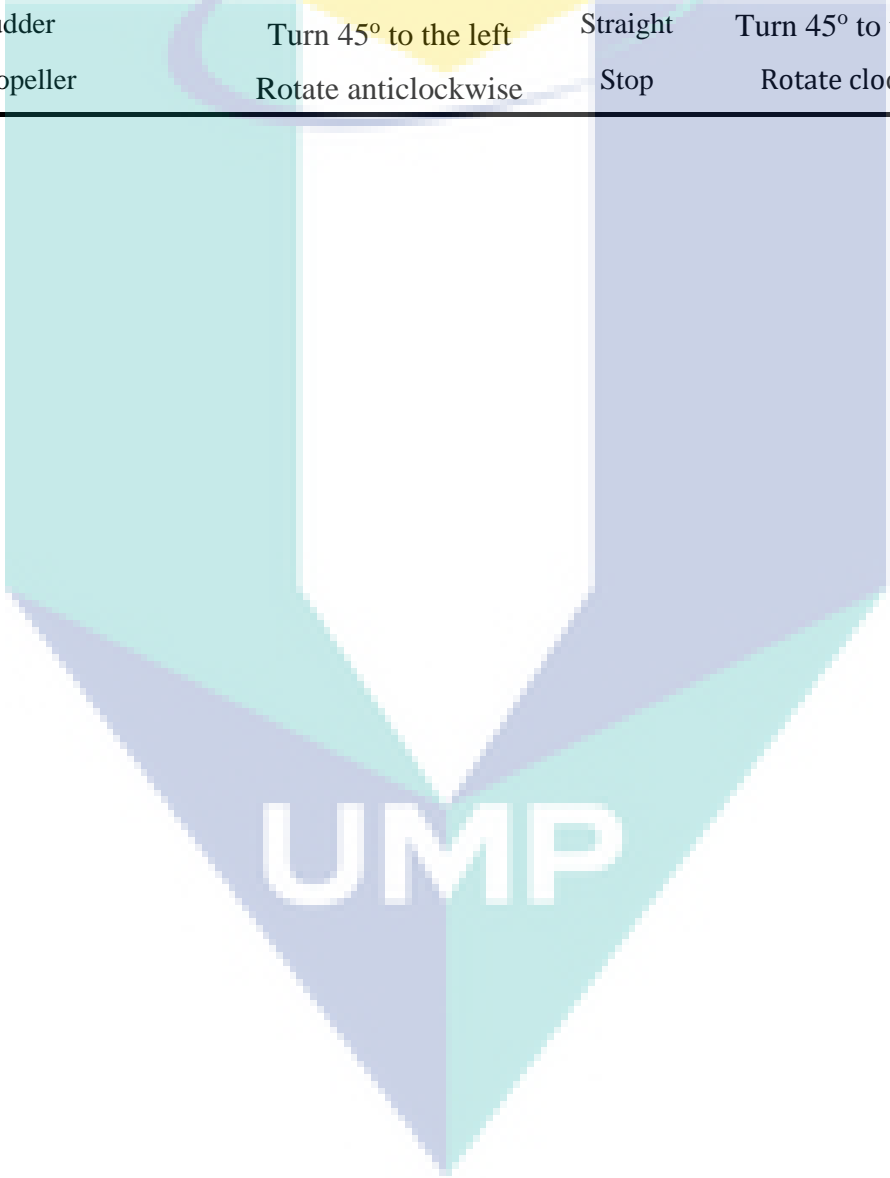
Figure 4-16 The motion of the internal sliding mass: (a) initial position, (b) Maximum position

The servo controller was tested in order to verify that the wings, rudder and propeller were able to function properly according to the provided PWM signal. The pulse length of the PWM signal was divided into three parts: 1.0 ms, 1.5 ms, 2.0 ms. If the 1.0 ms of pulse length is provided to the servo controller, the right wing turns 45° upward, the left wing turns 45° downward, the rudder turns 45° to the left side, and the

propeller produces maximum rotation speed in the anticlockwise direction. Table 4-4 shows the test results of the servo controller upon wings, rudder and propeller.

Table 4-4 Summary of controllers' performances

Actuators	Pulse length of PWM signal		
	1.0 ms	1.5 ms	2.0ms
Right wing	Turn 45° upward	Straight	Turn 45° downward
Left wing	Turn 45° downward	Straight	Turn 45° upward
Rudder	Turn 45° to the left	Straight	Turn 45° to the right
Propeller	Rotate anticlockwise	Stop	Rotate clockwise



CHAPTER 5

CONCLUSION

5.1 Conclusion

In this research work, three objectives have been set in Chapter 1. After completing all the works, all three objectives have been fulfilled. The QSMC was proposed for the linearised model. The proposed controller able to stabilise the output at the desired value with small steady state error. The performance of the QSMC was compared against LQR. From the comparison, QSMC had demonstrated the better performance as compared to LQR.

The prototype platform of the glider has been successfully developed and tested. The prototype of AUG has been developed according to the glider model. The prototype glider has been tested inside water tank. The real-time open-loop system test for the glider prototype has been performed in order to analyse the behaviour of the glider.

5.2 Recommendation

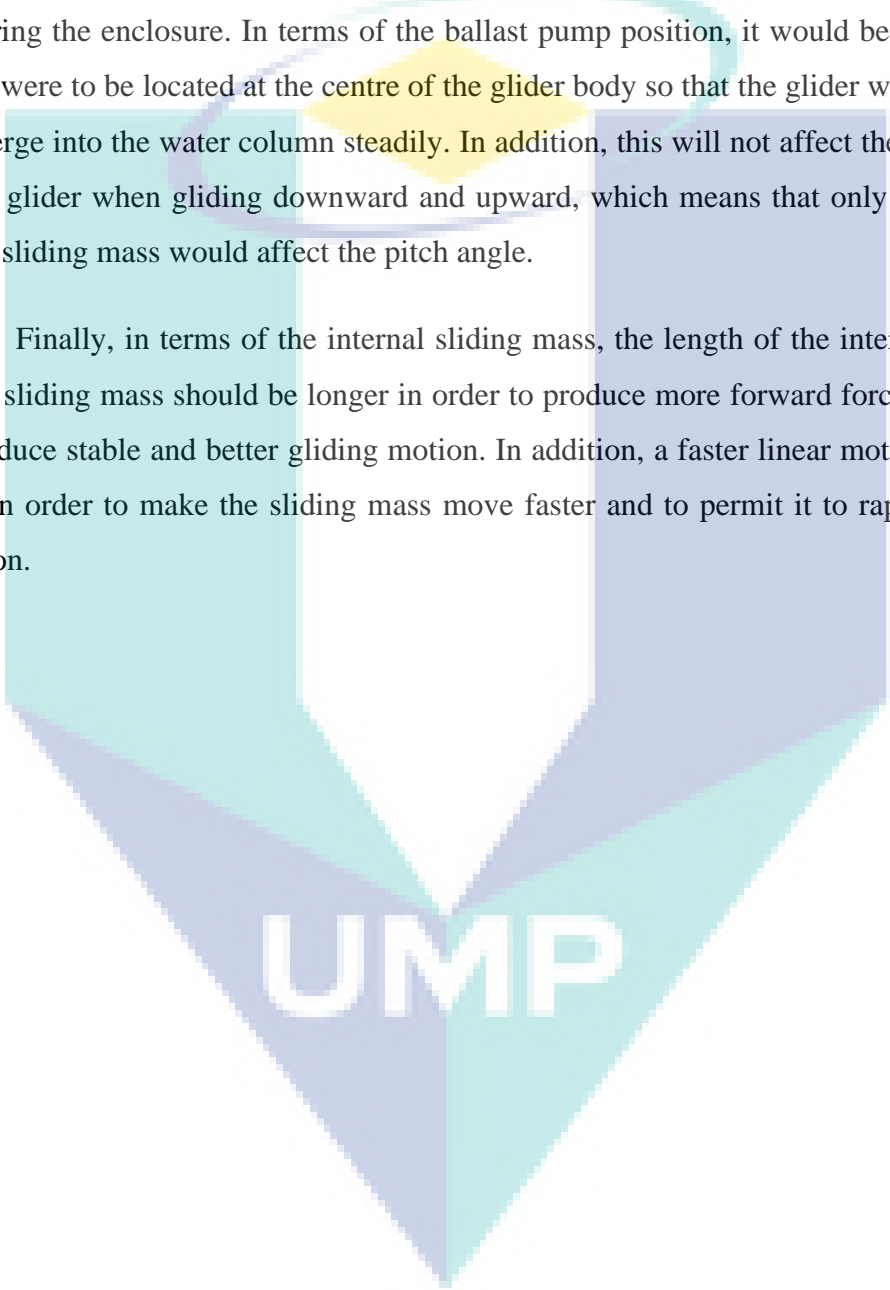
From the results and conclusions, improvements can be made to improve the performance of the proposed controllers. Therefore, several recommendations can be imposed for future works.

The first improvement is to optimise parameters of the controller. The optimisation can be done using any optimisation methods such as particle swarm optimisation, simulated Kalman filter and other available optimisation methods. In addition, various performance comparisons can be made with different optimisation methods to obtain the most optimised parameters of the controller. Secondly, the adaptive control can also be included in the proposed controller algorithm so that the controller has the adaptability to the disturbance of any other perturbations imposed to

the system. An observation based on controller can also be used so that with estimated states, it can reduce the control effort and chattering further.

For the glider design, several improvements could be made. In order to avoid a repetitive leakage problem on the servo motor enclosure, the underwater servo motor could be used to control the wings and rudder. Furthermore, this will reduce the cost of preparing the enclosure. In terms of the ballast pump position, it would be better if the pump were to be located at the centre of the glider body so that the glider will be able to submerge into the water column steadily. In addition, this will not affect the pitch angle of the glider when gliding downward and upward, which means that only the position of the sliding mass would affect the pitch angle.

Finally, in terms of the internal sliding mass, the length of the internal actuator of the sliding mass should be longer in order to produce more forward force, as well as to produce stable and better gliding motion. In addition, a faster linear motor should be used in order to make the sliding mass move faster and to permit it to rapidly change position.



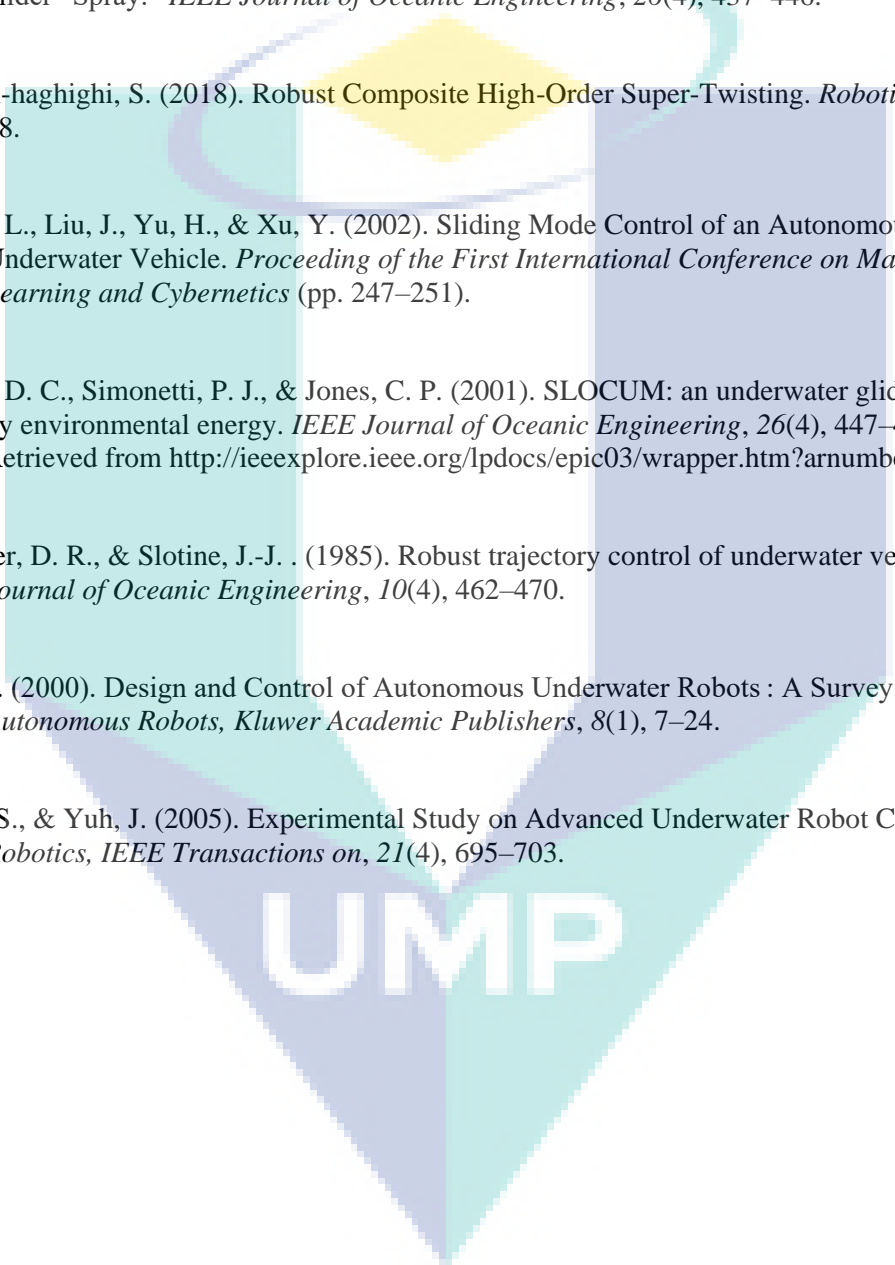
UMP

REFERENCES

- Bartolini, G., Ferrara, A., Levant, A., & Usai, E. (1999). On Second Order Sliding Mode Controllers. *Variable structure systems, sliding mode and nonlinear control*, 247, 329–350.
- Budiyono, A. (2009). Advances in unmanned underwater vehicles technologies : Modeling , control and guidance perspectives. *Indian Journal of Geo-Marine Sciences*, 38(3), 282–295.
- Burlion, L., Ahmed-Ali, T., & Seube, N. (2004). Glider's roll control based on back-stepping. *IFAC Proceedings Volumes*, 37(10), 161–165. Elsevier.
- Caiti, A., Calabrò, V., Geluardi, S., Grammatico, S., & Munafò, A. (2012). Switching control of an underwater glider with independently controllable wings. *IFAC Proceedings Volumes*, 45(27), 194–199.
- Cao, J., Cao, J., Zeng, Z., & Lian, L. (2016). Nonlinear multiple-input-multiple-output adaptive back-stepping control of underwater glider systems. *International Journal of Advanced Robotic Systems*, 13(6), 1–14.
- Cao, Jun liang, Yao, B. heng, & Lian, L. (2015). Nonlinear pitch control of an underwater glider based on adaptive back-stepping approach. *Journal of Shanghai Jiaotong University (Science)*, 20(6), 729–734.
- Dougherty, F., Sherman, T., Woolweaver, G., & Lovell, G. (1988). An autonomous underwater vehicle (AUV) flight control system using sliding mode control. *OCEANS '88. A Partnership of Marine Interests. Proceedings* (pp. 1265–1270 vol.4).
- Eriksen, C. C., Osse, T. J., Light, R. D., Wen, T., Lehman, T. W., Sabin, P. L., Ballard, J. W., et al. (2001). Seaglider: a long-range autonomous underwater vehicle for oceanographic research. *IEEE Journal of Oceanic Engineering*, 26(4), 424–436.
- Graver, J. G. (2005). *Underwater Gliders: Dynamics, Control and Design*. Princeton University.
- Graver, J., Liu, J., Woolsey, C., & Leonard, N. E. (1998). Design and Analysis of an Underwater Vehicle for Controlled Gliding. *32nd Conference on Information Sciences and Systems* (pp. 801–806). Princeton, USA.
- Healey, A. J., & Lienard, D. (1993). Multivariable sliding mode control for autonomous diving and steering of unmanned underwater vehicles. *Oceanic Engineering, IEEE Journal of*, 18(3), 327–339.

- Heng, C. T., Jamaludin, Z., Hashim, A. Y. B., Abdullah, L., & Rafan, N. A. (2017). Design of super twisting algorithm for chattering suppression in machine tools. *International Journal of Control, Automation and Systems*, 15(3), 1259–1266.
- Isa, K. (2015). *Homeostatic Inspired Controller Algorithm for a Hybrid-driven Autonomous Underwater Glider*. Universiti Sains Malaysia.
- Ismail, R. M. T. R., That, N. D., & Ha, Q. P. (2015). Automation in Construction Modelling and robust trajectory following for offshore container crane systems. *Automation in Construction*, 59, 179–187.
- Jalani, J., Herrmann, G., & Melhuish, C. (2010). Robust Trajectory Following for Underactuated Robot Fingers. *UKACC International Conference on Control 2010* (pp. 1–6). Coventry, UK.
- Kim, M., Joe, H., Kim, J., & Yu, S. (2015). Integral sliding mode controller for precise manoeuvring of autonomous underwater vehicle in the presence of unknown environmental disturbances. *International Journal of Control*, 88(March 2015), 1–43. Taylor & Francis.
- Leonard, N. E., & Graver, J. (2001). Model-based feedback control of autonomous underwater gliders. *IEEE Journal of Oceanic Engineering*, 26(4), 633–645.
- Levant, A. (1993). Sliding order and sliding accuracy in sliding mode control. *International Journal of Control*, 58(6), 1247–1263.
- Levant, A. (2007). Principles of 2-sliding mode design. *Automatica*, 43(4), 576–586.
- Levant, A., & Fridman, F. (2002). Higher Order Sliding Modes. In W. Perruquetti & J. P. Barbot (Eds.), *Sliding Mode Control in Engineering* (pp. 53–102). Taylor & Francis.
- Li, S., Member, S., Zhou, M., & Yu, X. (2013). Design and implementation of terminal sliding mode control method for PMSM speed regulation system. *IEEE Transactions on Industrial Informatics*, 9(4), 1879–1891.
- Mat-Noh, M., Mohd-Mokhtar, R., Arshad, M. R., Zain, Z. M., & Khan, Q. (2019). Review of sliding mode control application in autonomous underwater vehicles. *Indian Journal of Geo-Marine Sciences*, 48(7), 973–984.
- Md Zain, Z. (2012). *Underactuated Control for an Autonomous Underwater Vehicle with Four Thrusters*. Okayama University, Okayama, Japan.
- Rhif, A. (2012). Stabilizing sliding mode control design and application for DC motor: speed control. *International Journal of Instrumentation and Control Systems (IJICS)*, 2(1), 39–

- Salgado-Jimenez, T., & Jouvencel, B. (2003). Using a high order sliding modes for diving control a torpedo autonomous underwater vehicle. *Oceans 2003* (pp. 934–939). San diego, USA.
- Sherman, J., Davis, R. E., Owens, W. B., & Valdes, J. (2001). The autonomous underwater glider “Spray.” *IEEE Journal of Oceanic Engineering*, 26(4), 437–446.
- Tayebi-haghighi, S. (2018). Robust Composite High-Order Super-Twisting. *Robotics*, 7(1), 1–18.
- Wang, L., Liu, J., Yu, H., & Xu, Y. (2002). Sliding Mode Control of an Autonomous Underwater Vehicle. *Proceeding of the First International Conference on Machine Learning and Cybernetics* (pp. 247–251).
- Webb, D. C., Simonetti, P. J., & Jones, C. P. (2001). SLOCUM: an underwater glider propelled by environmental energy. *IEEE Journal of Oceanic Engineering*, 26(4), 447–452. Retrieved from <http://ieeexplore.ieee.org/lpdocs/epic03/wrapper.htm?arnumber=972077>
- Yoerger, D. R., & Slotine, J.-J. . (1985). Robust trajectory control of underwater vehicles. *IEEE Journal of Oceanic Engineering*, 10(4), 462–470.
- Yuh, J. (2000). Design and Control of Autonomous Underwater Robots : A Survey. *Autonomous Robots, Kluwer Academic Publishers*, 8(1), 7–24.
- Zhao, S., & Yuh, J. (2005). Experimental Study on Advanced Underwater Robot Control. *Robotics, IEEE Transactions on*, 21(4), 695–703.

The logo for UMP (Universidade do Maranhão) is a large, stylized letter 'U' composed of several overlapping geometric shapes in shades of blue, teal, and yellow. The letters 'UMP' are printed in a bold, white, sans-serif font across the center of the 'U' shape.

UMP

LIST OF PUBLICATIONS

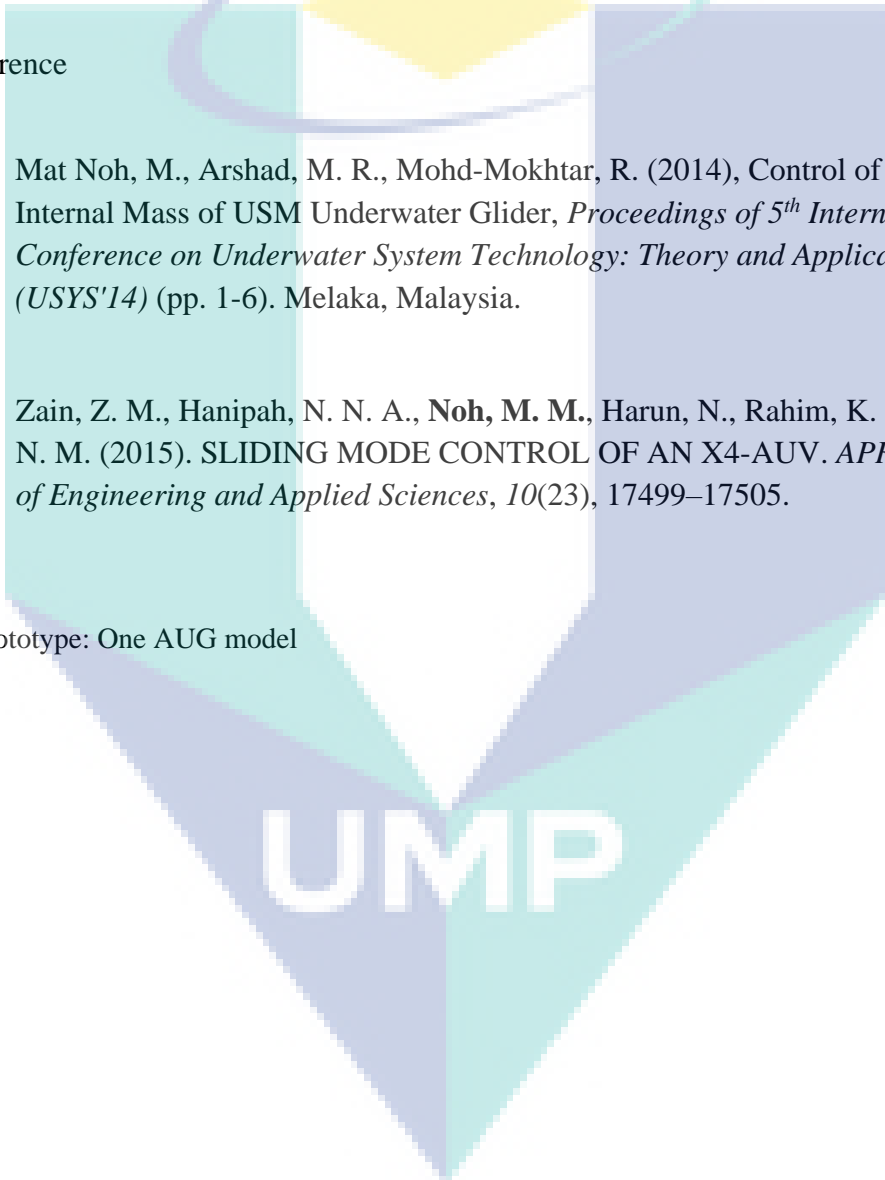
Journal

1. Mat Noh, M., Arshad, M. R., Mohd-Mokhtar, R. (2015). The evaluation of controller tracking performance based on Taylor's series expansion model, *Jurnal Teknologi*, 74:9 (2015). 175–181.

Conference

1. Mat Noh, M., Arshad, M. R., Mohd-Mokhtar, R. (2014), Control of 2DOF Internal Mass of USM Underwater Glider, *Proceedings of 5th International Conference on Underwater System Technology: Theory and Applications (USYS'14)* (pp. 1-6). Melaka, Malaysia.
2. Zain, Z. M., Hanipah, N. N. A., **Noh, M. M.**, Harun, N., Rahim, K. A. A., Zain, N. M. (2015). SLIDING MODE CONTROL OF AN X4-AUV. *APRN Journal of Engineering and Applied Sciences*, 10(23), 17499–17505.

Prototype: One AUG model



UMP